Biomedicine & Pharmacotherapy 166 (2023) 115295

Contents lists available at ScienceDirect

Biomedicine & Pharmacotherapy

journal homepage: www.elsevier.com/locate/biopha

# Antiproliferative activity and apoptosis-inducing mechanism of Amaryllidaceae alkaloid montanine on A549 and MOLT-4 human cancer cells

Darja Koutova [a], Negar Maafi [b], Darina Muthna [a], Karel Kralovec [c], Jana Kroustkova [b], Filip Pidany [b], Abdul Aziz Timbilla [a], Eva Cermakova [d], Lucie Cahlikova [b], Martina Rezacova [a], Radim Havelek [a,*,1]

[a] Department of Medical Biochemistry, Faculty of Medicine in Hradec Kralove, Charles University, Simkova 870, Hradec Kralove 500 03, Czech Republic
[b] ADINACO Research Group, Department of Pharmacognosy and Pharmaceutical Botany, Faculty of Pharmacy, Charles University, Heyrovskeho 1203, Hradec Kralove 500 05, Czech Republic
[c] Department of Biological and Biochemical Sciences, Faculty of Chemical Technology, University of Pardubice, Studentska 573, Pardubice 532 10, Czech Republic
[d] Department of Medical Biophysics, Faculty of Medicine in Hradec Kralove, Charles University, Simkova 870, Hradec Kralove 500 03, Czech Republic

ARTICLE INFO

*Keywords:*
Montanine
Manthine
Semisynthetic derivatives
Cytotoxicity
Apoptosis
Cell cycle arrest
DNA damage

ABSTRACT

The isoquinoline alkaloids found in Amaryllidaceae are attracting attention due to attributes that can be harnessed for the development of new drugs. The possible molecular mechanisms by which montanine exerts its inhibitory effects against cancer cells have not been documented. In the present study, montanine, manthine and a series of 15 semisynthetic montanine analogues originating from the parent alkaloid montanine were screened at a single test dose of 10 μM to explore their cytotoxic activities against a panel of eight cancer cell lines and one non-cancer cell line. Among montanine and its analogues, montanine and its derivatives **12** and **14** showed the highest cytostatic activity in the initial single-dose screening. However, the native montanine exhibited the greatest antiproliferative activity against cancer cells, with a lower mean $IC_{50}$ value of 1.39 μM, compared to the displayed mean $IC_{50}$ values of 2.08 μM for **12** and 3.57 μM for **14**. Montanine exhibited the most potent antiproliferative activity with $IC_{50}$ values of 1.04 μM and 1.09 μM against Jurkat and A549 cell lines, respectively. We also evaluated montanine's cytotoxicity and cell death mechanisms. Our results revealed that montanine triggered apoptosis of MOLT-4 cells via caspase activation, mitochondrial depolarisation and Annexin V/PI double staining. The Western blot results of MOLT-4 cells showed that the protein levels of phosphorylated Chk1 Ser345 were upregulated with increased montanine concentrations. Our findings provide new insights into the mechanisms underlying the cytostatic, cytotoxic and pro-apoptotic activities of montanine alkaloids in lung adenocarcinoma A549 and leukemic MOLT-4 cancer cell types.

*Abbreviations:* Akt, protein kinase B; BCA, bicinchoninic acid; CCCP, carbonyl cyanide 3-chlorophenylhydrazone; Cdc25A, cell division cycle 25 homolog A; Chk, checkpoint kinase; CI, cell index; DMSO, dimethyl sulfoxide; dsDNA, double-strand DNA; ECACC, European Collection of Cell Cultures; EDTA, ethylenediaminetetraacetic acid; ERK, extracellular regulated kinase; ESI-HRMS, electrospray ionization high resolution mass spectrometry; GP, growth percent; $IC_{50}$, half maximal inhibitory concentration; JC-1, 5′,6,6′-tetrachloro-1,1′,3,3′-tetraethylbenzimidazolylcarbocyanine iodide; MAPK, mitogen-activated protein kinase; MsCl, methanesulfonyl chloride; NSCLC, non-small cell lung cancer; p21/p27, inhibitor of cyclin dependent kinase; p53, tumor suppressor protein p53; PBS, phosphate buffered saline; PI, propidium iodide; ppm, parts per million; PVDF, polyvinylidene difluoride; Q-TOF, quadrupole-time-of-flight; ROS, reactive oxygen species; RTCA, real-time cell analysis; SD, standard deviation; ssDNA, single-strand DNA; TBS, Tris-buffered saline; TLC, thin layer chromatography; γH2AX, histon H2AX phosphorylated on Ser139; Δ Ψm, mitochondrial membrane potential.

* Corresponding author.
*E-mail address:* havelekr@lfhk.cuni.cz (R. Havelek).
[1] ORCID: 0000-0003-0528–1334

https://doi.org/10.1016/j.biopha.2023.115295
Received 23 May 2023; Received in revised form 2 August 2023; Accepted 4 August 2023
Available online 16 August 2023

## 1. Introduction

Plants produce a wide variety of secondary metabolites that play significant roles in disease prevention and treatment. Depending on their biosynthetic pathways, secondary plant compounds can be grouped into three major clusters: phenolics, terpenes and alkaloids [1]. Although alkaloids account for as much as 20% of all known secondary metabolites found in plants [2], only several plant-based alkaloids have been used as medications, either in their natural or semisynthetic forms [3]. Plant alkaloids can be used as lead compounds to design effective drug prototypes and pharmacological probes. Certain unaltered alkaloids and their derivatives have proven to be especially useful in drug development over the last few decades, and many alkaloid-inspired drugs are currently undergoing clinical trials for the potential treatment of various diseases [4,5]. A major proportion of such medications in clinical development are in the oncological field, and isoquinoline alkaloids (such as berberine) [6] or new analogues of blockbuster anticancer drugs based on camptothecin [7], vinblastine [8] or cephalotaxine-type skeletons [9] are employed.

In this context, isoquinoline-like alkaloid constituents of Amaryllidaceae plants have gained importance in the last few decades owing to growing interest in their potential medicinal use. Currently, approximately 600 naturally occurring alkaloids have been isolated from this plant family [10], some of which have been reported to have important biological and pharmacological effects [11–14]. These alkaloids can be further classified into nine different skeleton types (norbelladine, lycorine, homolycorine, galanthamine, haemanthamine, crinine, narciclasine, tazettine and montanine) and each has a relatively distinct bioactivity profile [10,12,13].

The montanine-type subclass constitutes a less abundant and limited group of alkaloids within the Amaryllidaceae, and 14 montanine-type alkaloids have been identified in the Amaryllidaceae species to date. Montanine-type alkaloids usually contain a C=C double bond substitution between C1 and C11a in the E ring of the 5,11-methanomorphanthridine skeleton, except for pancratinine B and pancratinine C, which have a double bond between C1 and C2 [12]. The representative structure of this group is montanine, which was among the first montanine-type skeleton alkaloids isolated from the *Haemanthus* species in 1955 [15]. Previous studies conducted on montanine-type alkaloids, pancracine [16–18], montanine [19–21], coccinine [20] and manthine [22] demonstrated a notable degree of in vitro cytotoxicity in cancer cells. However, little is known about the mechanisms underlying this cytotoxicity, and the only available information relates to pancracine levels. Recent investigations have demonstrated that pancracine is a potent inducer of apoptosis with upregulated activity of caspases − 3,− 7,− 8, and − 9 and increased protein levels of p53 phosphorylated at Ser392. Moreover, pancracine treatment perturbed cell cycle progression, causing G1-phase accumulation associated with the downregulation of Rb phosphorylated at Ser807/811 [18].

Many questions remain unanswered concerning the activity of montanine-type alkaloids, and it is necessary to deepen our mechanistic understanding of these. Montanine is not only the most active montanine-type structure, but it has also been shown to have the largest spectrum of anticancer potency in several in vitro models, including leukemia, lung, colon, pancreatic, ovarian, breast, osteosarcoma, melanoma and renal cancer [19–21]. Furthermore, because the 5,11-methanomorphanthridine scaffold is available for stereocentre modifications at C2 and C3 within ring E, montanine may be considered a valuable starting compound for semisynthesis and structure-activity relationship studies. As such observations have spurred investigations into further optimisation of the growth-inhibitory potency of montanine-type analogues, we considered it useful to synthesise, characterise and screen an array of montanine derivatives to determine their cytotoxic activity. In this respect, we reisolated montanine alkaloids from the bulbs of *Hippeastrum* taxa [21] in sufficient quantities to conduct semisynthetic structural modification. Manthine is another scant montanine-type alkaloid; we also included it in our study, and it was prepared using a previously described intramolecular rearrangement of the abundantly available Amaryllidaceae alkaloid haemanthamine [22]. We assayed the antiproliferative activities of montanine, manthine and 15 semisynthetic derivatives of montanine against a panel of nine cell lines of different histotypes. *In vitro* single-dose cytotoxicity screening showed that montanine, **12** with a 3-*O*-(3,5-dinitrobenzoyl) substitution at C3, **14** with a 3-*O*-(4-chloro-3-nitrobenzoyl) substitution at C3 and manthine displayed the most potent cytotoxicity. As native montanine exhibited the greatest antiproliferative activity among all the alkaloidal compounds tested, we investigated the effects of montanine on the growth or cell death of A549 and MOLT-4 cells to provide insights into the underlying mechanisms.

## 2. Materials and methods

### 2.1. General chemistry methods

All solvents were treated according to the standard techniques before use. All reagents and catalysts were purchased from a commercial source (Sigma-Aldrich, St. Louis, MO, USA) and used without further purification. The NMR spectra were acquired in $CDCl_3$ at ambient temperature on Jeol JNM-ECZ600R and Varian VNMR S500 spectrometers. The chemical shifts were recorded as $\delta$ values in parts per million (ppm) and were indirectly referenced to tetramethylsilane via the residual solvent signal ($CDCl_3$ - 7.26 ppm for $^1H$ and 77.0 ppm for $^{13}C$). Coupling constants ($J$) are in Hz. Electrospray ionization high resolution mass spectrometry (ESI-HRMS) were obtained utilizing a Waters Synapt G2-Si hybrid mass analyzer of a quadrupole-time-of-flight (Q-TOF) type, coupled to a Waters Acquity I-Class UHPLC system. The temperature program was: 100–180 °C at 15 °C/min, 1 min hold at 180 °C, and 180–300 °C at 5 °C /min and 5 min hold at 300 °C; detection range $m/z$ 40–600. The injector temperature was 280 °C. The flow-rate of the carrier gas (helium) was 0.8 mL/min. A split ratio of 1:15 was used. TLC was carried out on Merck precoated silica gel 60 F254 plates. The compounds on the plate were observed under UV light (254 and 366 nm) and visualized by spraying with Dragendorff's reagent.

### 2.2. General procedure for preparation of montanine esters (1−15)

Ester derivatives of montanine **1**–**15** (Fig. 1) have been prepared according to the procedure described previously [22]. The spectroscopic data for the already described derivatives (**13**–**15**) can be found in the following literature [22].

#### 2.2.1. 3-O-(3,5-dimethylbenzoyl)montanine (1)

Yield 26.8 mg (78%); pale yellow amorphous solid; $[\alpha]_D^{26} = -26.7°$ ($c$ 0.17, $CHCl_3$); $^1H$ NMR (500 MHz, $CDCl_3$) $\delta$: 7.56 – 7.52 (m, 2 H), 7.19 – 7.15 (m, 1 H), 6.60 (s, 1 H), 6.50 (s, 1 H), 5.90 (d, overlap, $J$ = 10.5 Hz, 1 H), 5.90 (d, overlap, $J$ = 10.5 Hz, 1 H), 5.63 – 5.58 (m, 1 H), 5.48 – 5.42 (m, 1 H), 4.37 (d, $J$ = 16.7 Hz, 1 H), 3.84 (d, $J$ = 16.7 Hz, 1 H), 3.68 – 3.63 (m, 1 H), 3.54 (s, 3 H), 3.47 – 3.40 (m, 1 H), 3.35 (d, $J$ = 2.5 Hz, 1 H), 3.12 (dd, $J$ = 11.4 Hz, $J$ = 2.5 Hz, 1 H), 3.07 (d, $J$ = 11.4 Hz, 1 H), 2.39 – 2.32 (m, 1 H), 2.32 (s, 6 H), 1.67 (td, $J$ = 12.0 Hz, $J$ = 3.2 Hz, 1 H); $^{13}C$ NMR (126 MHz, $CDCl_3$) $\delta$: 166.0, 154.7, 146.8, 146.0, 138.0, 134.7, 132.4, 130.0, 127.3, 124.8, 113.4, 107.4, 106.8, 100.7, 76.5, 71.3, 61.2, 58.8, 57.9, 55.3, 45.8, 30.2, 21.1; ESI-HRMS $m/z$ calcd for $C_{26}H_{28}NO_5^+$ $[M + H]^+$ 434.1962, found 434.1963.

#### 2.2.2. 3-O-(2,4,6-trimethylbenzoyl)montanine (2)

Yield 15.3 mg (50%); pale yellow amorphous solid; $[\alpha]_D^{22} = -3.2°$ ($c$ 0.51, $CHCl_3$); $^1H$ NMR (500 MHz, $CDCl_3$) $\delta$: 6.83 (s, 2 H), 6.54 (s, 1 H), 6.44 (s, 1 H), 5.88 (d, overlap, $J$ = 10.3 Hz, 1 H), 5.88 (d, overlap, $J$ = 10.3 Hz, 1 H), 5.61 – 5.54 (m, 1 H), 5.54 – 5.48 (m, 1 H), 4.34 (d, $J$ = 16.8 Hz, 1 H), 3.74 (d, $J$ = 16.8 Hz, 1 H), 3.64 – 3.61 (m, 1 H), 3.57 (s,

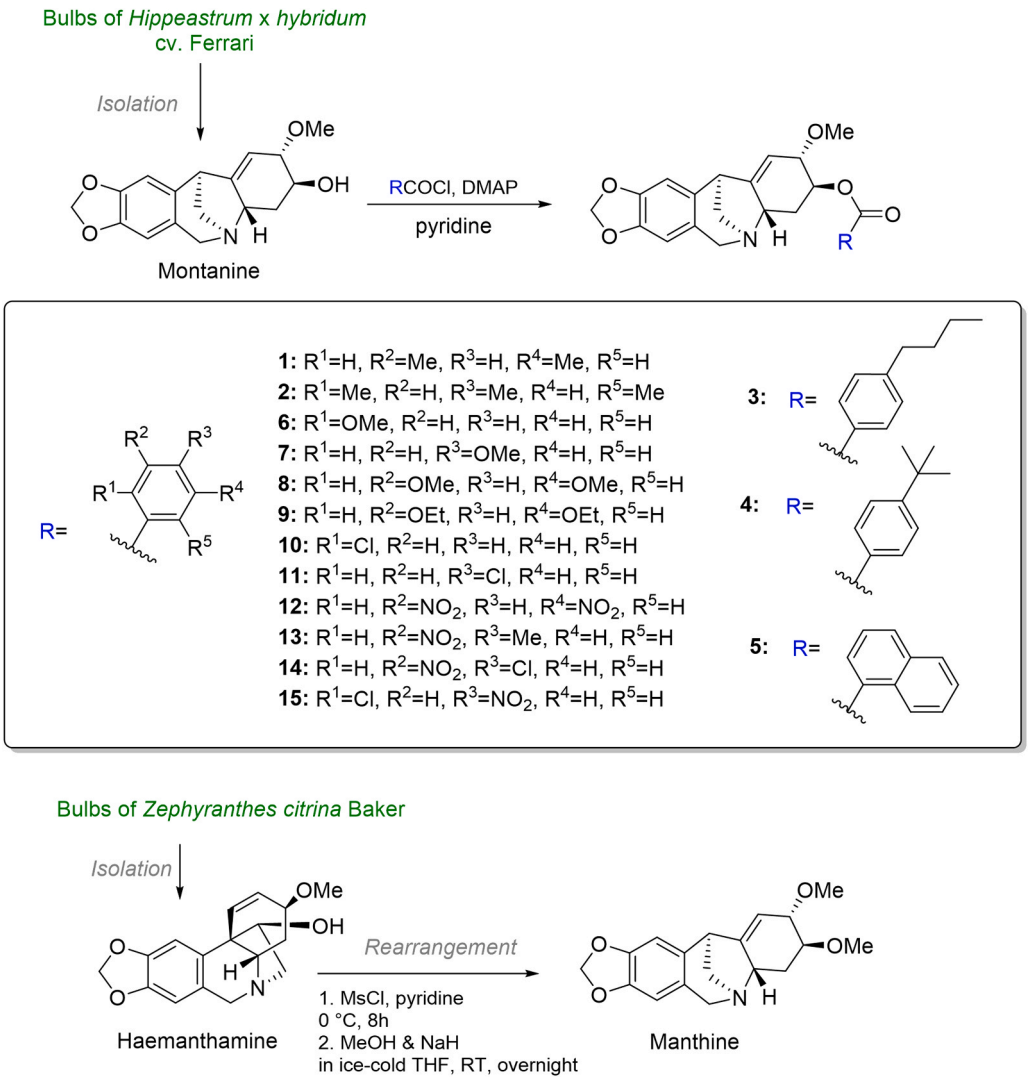


**Fig. 1.** Structures and synthetic routes for montanine derivatives (**1**–**15**) and manthine.

3 H), 3.38 – 3.32 (m, 1 H), 3.30 (d, $J$ = 2.5 Hz, 1 H), 3.10 (dd, $J$ = 11.1 Hz, $J$ = 2.5 Hz, 1 H), 3.04 (d, $J$ = 11.1 Hz, 1 H), 2.35 – 2.28 (m, 1 H), 2.27 (s, 3 H), 2.25 (s, 6 H), 1.73 – 1.64 (m, 1 H); $^{13}$C NMR (126 MHz, $CDCl_3$) $\delta$: 169.1, 154.6, 146.7, 146.0, 139.4, 135.0, 132.2, 130.7, 128.4, 124.6, 113.0, 107.3, 106.8, 100.7, 76.5, 71.1, 61.1, 58.6, 58.1, 55.4, 45.8, 29.9, 21.1, 19.7; ESI-HRMS $m/z$ calcd for $C_{27}H_{30}NO_5^+$ $[M + H]^+$ 448.2118, found 448.2122.

### 2.2.3. 3-O-(4-butylbenzoyl)montanine (3)

Yield 28.5 mg (100%); pale yellow amorphous solid; $[\alpha]_D^{30}$ = –15.0° ($c$ 0.16, $CHCl_3$); $^1$H NMR (600 MHz, $CDCl_3$) $\delta$: 7.86 – 7.80 (m, 2 H, AA′BB′), 7.22 – 7.17 (m, 2 H, AA′BB′), 6.57 (s, 1 H), 6.48 (s, 1 H), 5.90 – 5.87 (m, 2 H), 5.59 – 5.55 (m, 1 H), 5.46 – 5.42 (m, 1 H), 4.35 (d, $J$ = 16.7 Hz, 1 H), 3.82 (d, $J$ = 16.7 Hz, 1 H), 3.65 – 3.60 (m, 1 H), 3.52 (s, 3 H), 3.44 – 3.38 (m, 1 H), 3.32 (d, $J$ = 2.5 Hz, 1 H), 3.09 (dd, $J$ = 11.1 Hz, $J$ = 2.5 Hz, 1 H), 3.04 (d, $J$ = 11.1 Hz, 1 H), 2.65 – 2.60 (m, 2 H), 2.34 – 2.27 (m, 1 H), 1.65 (td, $J$ = 12.0 Hz, $J$ = 3.2 Hz, 1 H), 1.62 – 1.53 (m, 2 H), 1.34 – 1.27 (m, 2 H), 0.90 (t, $J$ = 7.4 Hz, 3 H); $^{13}$C NMR (151 MHz, $CDCl_3$) $\delta$: 165.7, 154.6, 148.7, 146.8, 146.0, 132.4, 129.7, 128.4, 127.5, 124.7, 113.4, 107.4, 106.8, 100.7, 76.5, 71.1, 61.1, 58.7, 58.0, 55.3, 45.9, 35.6, 33.2, 30.1, 22.2, 13.8; ESI-HRMS $m/z$ calcd for $C_{28}H_{32}NO_5^+$ $[M + H]^+$ 462.2275, found 462.2279.

### 2.2.4. 3-O-(4-tert-butylbenzoyl)montanine (4)

Yield 31.6 mg (100%); pale yellow amorphous solid; $[\alpha]_D^{26}$ = –25.1° ($c$ 0.18, $CHCl_3$); $^1$H NMR (600 MHz, $CDCl_3$) $\delta$: 7.89 – 7.83 (m, 2 H, AA′BB′), 7.43 – 7.38 (m, 2 H, AA′BB′), 6.57 (s, 1 H), 6.48 (s, 1 H), 5.90 – 5.87 (m, 2 H), 5.59 – 5.55 (m, 1 H), 5.47 – 5.42 (m, 1 H), 4.35 (d, $J$ = 16.8 Hz, 1 H), 3.82 (d, $J$ = 16.8 Hz, 1 H), 3.64 – 3.60 (m, 1 H), 3.52 (s, 3 H), 3.44 – 3.38 (m, 1 H), 3.32 (d, $J$ = 2.5 Hz, 1 H), 3.09 (dd, $J$ = 11.3 Hz, $J$ = 2.5 Hz, 1 H), 3.03 (d, $J$ = 11.3 Hz, 1 H), 2.33 – 2.27 (m, 1 H), 1.65 (td, $J$ = 11.9 Hz, $J$ = 3.1 Hz, 1 H), 1.30 (s, 9 H); $^{13}$C NMR (151 MHz, $CDCl_3$) $\delta$: 165.7, 156.8, 154.6, 146.8, 146.0, 132.4, 129.5, 127.3, 125.4, 124.7, 113.4, 107.4, 106.8, 100.7, 76.5, 71.0, 61.2, 58.7, 58.0, 55.3, 45.9, 35.1, 31.0, 30.1; ESI-HRMS $m/z$ calcd for $C_{28}H_{32}NO_5^+$ $[M + H]^+$ 462.2275, found 462.2279.

### 2.2.5. 3-O-(1-naphthoyl)montanine (5)

Yield 32.2 mg (100%); white amorphous solid; $[\alpha]_D^{22}$ = –59.5° ($c$ 0.52, $CHCl_3$); $^1$H NMR (600 MHz, $CDCl_3$) $\delta$: 8.72 (d, $J$ = 8.5 Hz, 1 H), 8.01 (dd, $J$ = 8.5 Hz, $J$ = 1.3 Hz, 1 H), 7.99 (d, $J$ = 8.5 Hz, 1 H), 7.84 (d, $J$ = 8.5 Hz, 1 H), 7.51 – 7.46 (m, 1 H), 7.46 – 7.38 (m, 2 H), 6.60 (s, 1 H), 6.46 (s, 1 H), 5.90 (d, overlap, $J$ = 8.3 Hz, 1 H), 5.90 (d, overlap, $J$ = 8.3 Hz, 1 H), 5.67 – 5.63 (m, 1 H), 5.59 – 5.54 (m, 1 H), 4.40 (d, $J$ = 16.7 Hz, 1 H), 3.86 (d, $J$ = 16.7 Hz, 1 H), 3.77 – 3.73 (m, 1 H), 3.60 (s, 3 H), 3.57 – 3.51 (m, 1 H), 3.40 (d, $J$ = 2.6 Hz, 1 H), 3.18 (dd, $J$ = 11.2 Hz, $J$ = 2.6 Hz, 1 H), 3.11 (d, $J$ = 11.2 Hz, 1 H), 2.51 – 2.44 (m,

1 H), 1.79 (td, $J = 12.7$ Hz, $J = 3.0$ Hz, 1 H); $^{13}$C NMR (126 MHz, $CDCl_3$) $\delta$: 166.7, 154.7, 146.8, 145.9, 133.8, 133.5, 132.3, 131.2, 130.2, 128.5, 127.7, 127.1, 126.2, 125.5, 124.7, 124.4, 113.3, 107.4, 106.9, 100.7, 76.2, 71.3, 61.1, 58.8, 58.1, 55.4, 45.8, 29.9; ESI-HRMS *m/z* calcd for $C_{28}H_{26}NO_5^+$ $[M + H]^+$ 456.1805, found 456.1810.

### 2.2.6. 3-O-(2-methoxylbenzoyl)montanine (6)

Yield 32.3 mg (73%); pale yellow amorphous solid; $[\alpha]_D^{22} = -42.6°$ (*c* 0.43, $CHCl_3$); $^1$H NMR (500 MHz, $CDCl_3$) $\delta$: 7.73 (dd, $J = 8.0$ Hz, $J = 1.8$ Hz, 1 H), 7.48 – 7.41 (m, 1 H), 6.98 – 6.92 (m, 1 H), 6.90 (d, $J = 8.0$ Hz, 1 H), 6.60 (s, 1 H), 6.49 (s, 1 H), 5.88 (d, overlap, $J = 9.2$ Hz, 1 H), 5.88 (d, overlap, $J = 9.2$ Hz, 1 H), 5.61 – 5.56 (m, 1 H), 5.49 – 5.43 (m, 1 H), 4.39 (d, $J = 16.7$ Hz, 1 H), 3.85 (d, $J = 16.7$ Hz, 1 H), 3.67 – 3.63 (m, 1 H), 3.61 (s, 3 H), 3.59 – 3.51 (m, overlap, 1 H), 3.56 (s, overlap, 3 H), 3.35 (d, $J = 2.5$ Hz, 1 H), 3.14 (dd, $J = 11.2$ Hz, $J = 2.5$ Hz, 1 H), 3.07 (d, $J = 11.2$, 1 H), 2.39 – 2.31 (m, 1 H), 1.68 (td, $J = 13.1$ Hz, $J = 2.7$ Hz, 1 H); $^{13}$C NMR (126 MHz, $CDCl_3$) $\delta$: 165.6, 159.2, 154.3, 146.7, 146.0, 133.7, 132.4, 131.8, 124.6, 120.1, 119.8, 113.2, 111.9, 107.5, 106.7, 100.7, 75.9, 70.6, 61.1, 58.8, 58.1, 55.5, 45.8, 29.5; ESI-HRMS *m/z* calcd for $C_{25}H_{26}NO_6^+$ $[M + H]^+$ 436.1755, found 436.1764.

### 2.2.7. 3-O-(4-methoxybenzoyl)montanine (7)

Yield 30.0 mg (74%); pale yellow amorphous solid; $[\alpha]_D^{22} = -30.4°$ (*c* 0.50, $CHCl_3$); $^1$H NMR (500 MHz, $CDCl_3$) $\delta$: 7.94 – 7.87 (m, 2 H, AA′BB′), 6.93 – 6.86 (m, 2 H, AA′BB′), 6.60 (s, 1 H), 6.51 (s, 1 H), 5.93 – 5.89 (m, 2 H), 5.62 – 5.57 (m, 1 H), 5.48 – 5.42 (m, 1 H), 4.37 (d, $J = 16.8$ Hz, 1 H), 3.85 (s, overlap, 3 H), 3.85 (d, overlap, $J = 16.8$ Hz, 1 H), 3.67 – 3.61 (m, 1 H), 3.55 (s, 3 H), 3.46 – 3.39 (m, 1 H), 3.34 (d, $J = 2.5$ Hz, 1 H), 3.12 (dd, $J = 11.5$ Hz, $J = 2.5$ Hz, 1 H), 3.05 (d, $J = 11.5$ Hz, 1 H), 2.36 – 2.28 (m, 1 H), 1.66 (td, $J = 12.0$ Hz, $J = 3.1$ Hz, 1 H); $^{13}$C NMR (126 MHz, $CDCl_3$) $\delta$: 165.4, 163.4, 154.6, 146.7, 145.9, 132.4, 131.7, 124.7, 122.4, 113.6, 113.4, 107.4, 106.8, 100.8, 76.4, 70.9, 61.1, 58.7, 58.0, 55.4, 55.3, 45.9, 30.1; ESI-HRMS *m/z* calcd for $C_{25}H_{26}NO_6^+$ $[M + H]^+$ 436.1755, found 436.1760.

### 2.2.8. 3-O-(3,5-dimethoxybenzoyl)montanine (8)

Yield 29.3 mg (71%); pale yellow amorphous solid; $[\alpha]_D^{26} = -35.9°$ (*c* 0.15, $CHCl_3$); $^1$H NMR (500 MHz, $CDCl_3$) $\delta$: 7.06 (d, $J = 2.4$ Hz, 2 H), 6.62 (t, $J = 2.4$ Hz, 1 H), 6.59 (s, 1 H), 6.48 (s, 1 H), 5.90 (d, overlap, $J = 9.1$ Hz, 1 H), 5.89 (d, overlap, $J = 9.1$ Hz, 1 H), 5.62 – 5.57 (m, 1 H), 5.47 – 5.42 (m, 1 H), 4.37 (d, $J = 16.8$ Hz, 1 H), 3.83 (d, $J = 16.8$ Hz, 1 H), 3.74 (s, 6 H), 3.66 – 3.59 (m, 1 H), 3.54 (s, 3 H), 3.48 – 3.41 (m, 1 H), 3.33 (d, $J = 2.4$ Hz, 1 H), 3.12 (dd, $J = 11.3$ Hz, $J = 2.4$ Hz, 1 H), 3.07 (d, $J = 11.3$ Hz, 1 H), 2.37 – 2.29 (m, 1 H), 1.73 – 1.64 (m, 1 H); $^{13}$C NMR (126 MHz, $CDCl_3$) $\delta$: 165.3, 160.5, 154.6, 146.8, 146.0, 132.3, 132.0, 124.6, 113.1, 107.4, 107.2, 106.8, 105.7, 100.7, 76.2, 71.4, 61.2, 58.7, 58.0, 55.4, 45.8, 29.9; ESI-HRMS *m/z* calcd for $C_{26}H_{28}NO_7^+$ $[M + H]^+$ 466.1860, found 466.1866.

### 2.2.9. 3-O-(3,5-diethoxybenzoyl)montanine (9)

Yield 9.03 mg (28%); pale yellow amorphous solid; $[\alpha]_D^{21} = -34.3°$ (*c* 0.11, $CHCl_3$); $^1$H NMR (500 MHz, $CDCl_3$) $\delta$: 7.05 (d, $J = 2.3$ Hz, 2 H), 6.61 (t, $J = 2.3$ Hz, 1 H), 6.59 (s, 1 H), 6.48 (s, 1 H), 5.90 (d, overlap, $J = 9.3$ Hz, 1 H), 5.90 (d, overlap, $J = 9.3$ Hz, 1 H), 5.61 – 5.57 (m, 1 H), 5.47 – 5.42 (m, 1 H), 4.37 (d, $J = 16.8$ Hz, 1 H), 3.97 (q, $J = 7.0$ Hz, 4 H), 3.83 (d, $J = 16.8$ Hz, 1 H), 3.67 – 3.59 (m, 1 H), 3.53 (s, 3 H), 3.46 – 3.40 (m, 1 H), 3.34 (d, $J = 2.5$ Hz, 1 H), 3.12 (dd, $J = 11.4$ Hz, $J = 2.5$ Hz, 1 H), 3.07 (d, $J = 11.4$ Hz, 1 H), 2.36 – 2.28 (m, 1 H), 1.71 – 1.62 (m, 1 H), 1.39 (t, $J = 7.0$ Hz, 6 H); $^{13}$C NMR (126 MHz, $CDCl_3$) $\delta$: 165.5, 159.9, 154.6, 146.8, 146.0, 132.3, 131.9, 124.7, 113.2, 107.7, 107.5, 106.8, 106.5, 100.8, 76.3, 71.4, 63.7, 61.2, 58.7, 58.0, 55.4, 45.8, 30.0, 14.7; ESI-HRMS *m/z* calcd for $C_{28}H_{32}NO_7^+$ $[M + H]^+$ 494.2173, found 494.2178.

### 2.2.10. 3-O-(2-chlorobenzoyl)montanine (10)

Yield 19.8 mg (86%); yellow amorphous solid; $[\alpha]_D^{21} = -37.6°$ (*c* 0.45, $CHCl_3$); $^1$H NMR (600 MHz, $CDCl_3$) $\delta$: 7.73 – 7.68 (m, 1 H), 7.41 – 7.31 (m, 2 H), 7.31 – 7.24 (m, 1 H), 6.55 (s, 1 H), 6.46 (s, 1 H), 5.88 (d, overlap, $J = 9.5$ Hz, 1 H), 5.88 (d, overlap, $J = 9.5$ Hz, 1 H), 5.60 – 5.55 (m, 1 H), 5.49 – 5.45 (m, 1 H), 4.36 (d, $J = 16.7$ Hz, 1 H), 3.81 (d, $J = 16.7$ Hz, 1 H), 3.67 – 3.61 (m, 1 H), 3.54 (s, 3 H), 3.52 – 3.47 (m, 1 H), 3.33 (d, $J = 2.6$ Hz, 1 H), 3.12 (dd, $J = 11.2$ Hz, $J = 2.6$ Hz, 1 H), 3.05 (d, $J = 11.2$, 1 H), 2.41 – 2.32 (m, 1 H), 1.69 (td, $J = 12.0$ Hz, $J = 3.0$ Hz, 1 H); $^{13}$C NMR (151 MHz, $CDCl_3$) $\delta$: 165.1, 154.1, 146.8, 146.1, 133.5, 132.6, 132.1, 131.4, 131.0, 130.3, 126.6, 124.3, 113.2, 107.4, 106.8, 100.8, 76.0, 72.0, 61.0, 58.8, 58.1, 55.4, 45.7, 29.6; ESI-HRMS *m/z* calcd for $C_{24}H_{23}ClNO_5^+$ $[M + H]^+$ 440.1259, found 440.1264.

### 2.2.11. 3-O-(4-chlorobenzoyl)montanine (11)

Yield 18.5 mg (75%); yellow amorphous solid; $[\alpha]_D^{21} = -29.3°$ (*c* 0.53, $CHCl_3$); $^1$H NMR (600 MHz, $CDCl_3$) $\delta$: 7.88 – 7.82 (m, 2 H, AA′BB′), 7.39 – 7.31 (m, 2 H, AA′BB′), 6.58 (s, 1 H), 6.49 (s, 1 H), 5.91 – 5.86 (m, 2 H), 5.61 – 5.57 (m, 1 H), 5.46 – 5.41 (m, 1 H), 4.38 (d, $J = 16.7$ Hz, 1 H), 3.84 (d, $J = 16.7$ Hz, 1 H), 3.64 – 3.60 (m, 1 H), 3.52 (s, 3 H), 3.43 – 3.37 (m, 1 H), 3.35 (d, $J = 2.9$ Hz, 1 H), 3.11 (dd, $J = 11.0$ Hz, $J = 2.9$ Hz, 1 H), 3.06 (d, $J = 11.0$ Hz, 1 H), 2.37 – 2.30 (m, 1 H), 1.68 (td, $J = 12.0$ Hz, $J = 3.2$ Hz, 1 H); $^{13}$C NMR (151 MHz, $CDCl_3$) $\delta$: 164.8, 154.1, 146.9, 146.1, 139.6, 132.1, 131.0, 128.7, 128.5, 124.3, 113.6, 107.4, 106.9, 100.8, 76.3, 71.6, 61.0, 58.8, 58.0, 55.3, 45.8, 29.9; ESI-HRMS *m/z* calcd for $C_{24}H_{23}ClNO_5^+$ $[M + H]^+$ 440.1259, found 440.1266.

### 2.2.12. 3-O-(3,5-dinitrobenzoyl)montanine (12)

Yield 10.1 mg (20%); intense yellow amorphous solid; $[\alpha]_D^{22} = -21.1°$ (*c* 0.10, $CHCl_3$); $^1$H NMR (500 MHz, $CDCl_3$) $\delta$: 9.21 (t, $J = 2.2$ Hz, 1 H), 9.05 (d, $J = 2.2$ Hz, 2 H), 6.59 (s, 1 H), 6.52 (s, 1 H), 5.91 (d, overlap, $J = 11.9$ Hz, 1 H), 5.91 (d, overlap, $J = 11.9$ Hz, 1 H), 5.67 – 5.62 (m, 1 H), 5.54 – 5.49 (m, 1 H), 4.40 (d, $J = 16.8$ Hz, 1 H), 3.85 (d, $J = 16.8$ Hz, 1 H), 3.74 – 3.70 (m, 1 H), 3.55 (s, 3 H), 3.45 – 3.39 (m, 1 H), 3.38 (d, $J = 2.2$ Hz, 1 H), 3.13 (dd, $J = 11.3$ Hz, $J = 2.2$ Hz, 1 H), 3.10 (d, $J = 11.3$ Hz, 1 H), 2.43 – 2.35 (m, 1 H), 1.77 (td, $J = 12.0$ Hz, $J = 3.4$ Hz, 1 H); $^{13}$C NMR (126 MHz, $CDCl_3$) $\delta$: 161.8, 154.7, 148.6, 147.0, 146.2, 133.7, 132.0, 129.5, 124.5, 122.5, 112.9, 107.3, 106.9, 100.9, 76.2, 74.3, 61.2, 58.7, 58.0, 55.3, 45.8, 30.2; ESI-HRMS *m/z* calcd for $C_{24}H_{22}N_3O_9^+$ $[M + H]^+$ 496.1351, found 496.1358.

## 2.3. Preparation of manthine

Manthine was synthesized through the rearrangement of haemanthamine, as described by Govindaraju et al. [22]. To 100 mg of haemanthamine dissolved in 3 mL of dry pyridine, 100 μL of methanesulfonyl chloride (MsCl) was added and the reaction mixture was stirred at 0 °C for 8 h. After an hour of standing at 25 °C, the reaction mixture was added into a solution of ice-cold THF (3 mL) and methanol (25 μL) pre-treated with 60 mg NaH. The mixture was left stirring overnight, and afterward, 10 mL of water was poured into the reaction mixture and subsequently extracted with $CHCl_3$ (2 × 20 mL). The combined organic phases were dried over $Na_2SO_4$, filtered, and then the solvent was removed under reduced pressure. The residue was purified by preparative TLC (To:$Et_2NH$ 9:1), furnishing 64.5 mg of manthine (61%) as a pale yellow amorphous solid. Our spectroscopic data for manthine corresponds with previously published descriptions [24].

Yield 64.5 mg (61%); pale yellow amorphous solid; $[\alpha]_D^{21} = -54.7°$ (*c* 0.47, $CHCl_3$); $^1$H NMR (500 MHz, $CDCl_3$) $\delta$: 6.54 (s, 1 H), 6.46 (s, 1 H), 5.87 (d, overlap, $J = 13.0$, 1 H), 5.87 (d, overlap, $J = 13.0$, 1 H), 5.58 – 5.53 (m, 1 H), 4.34 (d, $J = 16.6$ Hz, 1 H), 3.81 (d, $J = 16.6$ Hz, 1 H), 3.63 – 3.57 (m, 1 H), 3.57 – 3.52 (m, 1 H), 3.44 (s, 3 H), 3.39 (s, 3 H), 3.33 – 3.28 (m, 1 H), 3.27 (d, $J = 2.7$ Hz, 1 H), 3.07 (dd, $J = 11.0$ Hz, $J = 2.7$ Hz, 1 H), 3.03 (d, $J = 11.0$ Hz, 1 H), 2.33 – 2.25 (m, 1 H), 1.42 (td, $J = 12.5$ Hz, $J = 3.0$ Hz, 1 H); $^{13}$C NMR (126 MHz, $CDCl_3$) $\delta$: 154.6, 146.7,

145.9, 132.5, 124.9, 112.8, 107.4, 106.8, 100.7, 78.0, 76.6, 61.1, 58.4, 57.3, 56.6, 55.4, 45.8, 29.5; ESI-HRMS *m/z* calcd for $C_{18}H_{22}NO_4^+$ $[M + H]^+$ 316.1543, found 316.1543.

### 2.4. Cell culture and culture conditions

The human derived acute T cell leukemia (Jurkat; catalogue code: 88042803), acute lymphoblastic leukemia (MOLT-4; catalogue code: 85011413), lung adenocarcinoma (A549; catalogue code: 86012804), colorectal adenocarcinoma (HT-29; catalogue code: 85061109), pancreatic epithelioid carcinoma (PANC-1; catalogue code: 87092802), ovarian carcinoma (A2780; catalogue code: 93112519), breast adenocarcinoma (MCF-7; catalogue code: 86012803), osteosarcoma (SAOS-2; catalogue code: 89050205), hepatocellular carcinoma (HepG2; catalogue code: 85011430), melanoma (A375; catalogue code: 88113005), and normal lung fibroblasts (MRC-5; catalogue code: 05072101) cell lines were purchased from European Collection of Authenticated Cell Cultures (ECACC, Salisbury, UK) and cultured according to the provider's culture method guidelines. The cells were subcultured at 37 °C in a humidified incubator with 5% carbon dioxide and 95% air. The cells with a low passage number (non-tumor primary cell line MRC-5 was used for a maximum of 10 passages and cancer cell lines were used for a maximum of 20 passages) and in an exponential growth phase were used for this study. The cell lines were periodically tested for mycoplasma contamination.

### 2.5. Cell treatment

Fresh stock solutions of montanine, manthine and derivatives with aromatic ring **1** – **15** in concentrations of 50 mM were dissolved in dimethyl sulfoxide (DMSO) (Sigma-Aldrich, St. Louis, MO, USA). Stock solutions were freshly prepared before use. For the experiments, the stock solutions were diluted with the complete culture medium to create final concentrations of 1–50 μM (50 μM was the highest concentration used in xCELLigence measurement), making sure that the concentration of DMSO was $< 0.1\%$ to avoid toxic effects on the cells. Negative control cells were sham treated with a DMSO vehicle only (0.1%; control). Cells treated with 5% DMSO, CCCP - carbonyl cyanide 3-chlorophenylhydrazone (Life Technologies, Grand Island, NY, USA) at 50 μM, menadione (Sigma-Aldrich, St. Louis, MO, USA) at 50 μM, cisplatin (Sigma-Aldrich, St. Louis, MO, USA) at 5 μM or doxorubicin (Sigma-Aldrich, St. Louis, MO, USA) at 0.25 μM and 1 μM were used as a positive control.

### 2.6. Screening for antiproliferative activity, growth percent and $IC_{50}$ value calculation

In starting experiments, each cell line was seeded at a previously established optimal density ($1 \times 10^3$ to $50 \times 10^3$ cells per well) in a 96-well plate (TPP, Trasadingen, Switzerland) and cells were allowed to settle overnight. Cells were treated for 48 h with alkaloids in either a final concentration of 10 μM or in a broad concentration range of 0.1–100 μM (determination of $IC_{50}$ values). Doxorubicin (Sigma-Aldrich, St. Louis, USA), at a concentration of 1 μM, was used as a positive control. At the end of the cultivation period, the WST-1 proliferation assay (Sigma-Aldrich, St. Louis, USA) was performed according to the manufacturer's protocol and the absorbance was measured using Tecan Spark (Tecan, Männedorf, Switzerland). Each value is the mean of experiments that were repeated independently for a minimum of three times and represents the percentage of proliferation of 0.1% DMSO mock treated control cells (100%). The growth percent (GP) value was calculated for each alkaloid tested. GP represents the mean of the proliferation decrease in percent of all the 9 cell lines treated with the same alkaloid.

### 2.7. Screening for antiproliferative activity using the xCELLigence system

The xCELLigence system (Roche, Basel, Switzerland and ACEA Biosciences, San Diego, CA, USA) was used to monitor cell adhesion, proliferation, and cytotoxicity. It was connected and tested by Resistor Plate before the RTCA SP (single plate) station was placed inside the incubator at 37 °C with an atmosphere containing 5% $CO_2$. First, the seeding concentration for the experiments was optimized for each cell line. After seeding, the respective number of cells in 190 μL of medium per well of the E-plate 96, and the proliferation, attachment and spreading of the cells were monitored every 30 min by the xCELLigence system. Approximately 24 h after seeding, when the cells were in the log growth phase, they were exposed in triplicates to 10 μL of sterile deionized water containing montanine to obtain final concentrations of 1 – 50 μM. Controls received sterile deionized water + DMSO with a final concentration of 0.1%. Cells treated with 5% DMSO were used as a positive control. Growth curves were normalized to the time point of treatment. Evaluations were performed using xCELLigence 1.2.1 software (Roche, Basel, Switzerland and ACEA Biosciences, San Diego, CA, USA).

### 2.8. Proliferation and viability measurement using Trypan blue exclusion assay

A Trypan blue exclusion assay was used for measuring cell proliferation and viability. The cells were treated with varying concentrations of the montanine and further cultured for 24, 48 and 72 h in the case of A549 cells, and 24 and 48 h in the case of MOLT-4 cells. Cells treated with 0.25 μM doxorubicin were used as a positive control. Cell membrane integrity was determined using the Trypan blue exclusion technique – mixing 50 μL of 0.5% Trypan blue and 50 μL of cell suspension. In case of A549 adherent-culture cells, floating cells were pooled with adherent cells that had been trypsinized and resuspended in medium before being mixed with 0.5% Trypan blue. Cell counts were carried out using a Bürker chamber and a Nikon Eclipse E200 light microscope (Nikon, Tokyo, Japan).

### 2.9. Cell cycle and internucleosomal DNA fragmentation analysis

Cultured cells were harvested by trypsinization, collected, washed with ice-cold PBS, fixed with 70% ethanol and stored at 4 °C for subsequent cell cycle distribution analysis. Afterward, fixed cells were centrifuged to remove ethanol and washed with ice-cold PBS twice. In order to detect low molecular-weight fragments of DNA, the cells were incubated for 5 min at room temperature in a buffer (192 mL 0.2 M $Na_2HPO_4$ + 8 mL of 0.1 M citric acid, pH 7.8) and then, after washing cells with ice-cold PBS, labelled with propidium iodide in Vindelov's solution for 1 h at 37 °C. The DNA content was determined by using a CytoFLEX LX flow cytometer by Beckman Coulter with an excitation wavelength of 488 nm and emission spectrum 600–620 nm. The data were analysed using Kaluza Analysis 2.1 software.

### 2.10. Activity of caspases

The caspase-dependent induction of programmed cell death was determined by monitoring the activities of caspases-3/7, caspase-8 and caspase-9 by Caspase-Glo Assays (Promega, Madison, WI, USA) 24 h after treatment with 2, 5 and 10 μM of montanine. Cells treated with 1 μM of doxorubicin were used as a positive control. The assay provides a proluminogenic substrate in an optimized buffer system. The addition of a Caspase-Glo Reagent results in cell lysis, followed by caspase cleavage of the substrate and the generation of a luminescent signal. A total of $1 \times 10^4$ cells was seeded per well using a 96-well-plate format (Sigma-Aldrich, St. Louis, MO, USA). After treatment, the Caspase-Glo Assay Reagent was added to each well (50 μL/well) and incubated for 30 min before luminescence was measured using a Tecan Spark multimode microplate reader (Tecan Group, Männedorf, Switzerland).

### 2.11. Annexin V/PI flow cytometry analysis of apoptosis

Apoptosis was determined by flow cytometry using an Alexa Fluor® 488 Annexin V/Dead Cell Apoptosis kit (Life Technologies, Grand Island, NY, USA) in accordance with the manufacturer's instructions. The Alexa Fluor®488 Annexin V/Dead Cell Apoptosis kit employs the property of Alexa Fluor®488 conjugated to Annexin V to bind to phosphatidylserine in the presence of $Ca^{2+}$; and the ability of propidium iodide (PI) to enter cells with damaged cell membranes and bind to DNA. For each sample, a minimum of 20 000 events were acquired using a CytoFLEX LX Flow Cytometer (Beckman Coulter, Miami, FL, USA). List mode data were analysed using Kaluza Analysis 2.1 software (Beckman Coulter, Miami, FL, USA).

### 2.12. Measurement of mitochondrial membrane potential

The loss of the mitochondrial membrane potential (Δ Ψm) was quantitatively determined by flow cytometry using a MitoProbe™ JC-1 Assay Kit (Life Technologies, Grand Island, NY, USA). JC-1 (5′,6,6′-tetrachloro-1,1′,3,3′-tetraethylbenzimidazolylcarbocyanine iodide) is a cationic dye that exhibits potential-dependent accumulation in mitochondria, indicated by a fluorescence emission shift from green monomeric (~529 nm) to orange-red J-aggregate (~590 nm) forms. Apoptosis results in a breakdown of the mitochondrial membrane potential with a subsequent shift from orange-red (aggregates) to green (monomers) fluorescence. The procedures of the JC-1 assay were performed according to the manufacturer's instructions. Briefly, approximately $1 \times 10^6$ cells from each condition were collected, washed with Dulbecco's phosphate-buffered saline (DPBS), and resuspended in a complete medium at a concentration of $6 \times 10^5$ cells/mL. Cells incubated with carbonyl cyanide 3-chlorophenylhydrazone (CCCP) at a final concentration 50 μM were used as a positive control of mitochondrial membrane depolarization. The cells were stained with 2 μM final concentration of JC-1 and incubated in the dark at 37 °C for 30 min. Fluorescence was measured using a CytoFLEX LX Flow Cytometer (Beckman Coulter, Miami, FL, USA). List mode data were analysed using Kaluza Analysis 2.1 software (Beckman Coulter, Miami, FL, USA).

### 2.13. Immunofluorescence staining of γH2AX and epi-fluorescence microscopy

For each condition, $1 \times 10^5$ MOLT-4 cells seeded in 1-well chamber slides (Nunc, Langenselbold, Germany) were fixed with 4% freshly prepared paraformaldehyde for 10 min at room temperature, washed with PBS, and permeabilized in 0.2% Triton X-100/PBS. Cells were blocked in a solution with 7% FCS and 2% BSA and immunostained with a γH2AX primary antibody (Cell Signaling, Boston, MA, USA) overnight at 4 °C. The secondary Cy™3-conjugated antibody (Jackson ImmunoResearch Labarotories, West Grove, PA, USA) was applied to each slide (after their preincubation with 5.5% donkey serum in PBS for 30 min at room temperature), and incubation for 1 h in the dark was succeeded by washing (3 ×5 min) in PBS. The nuclei were counterstained using a DAPI solution (Sigma-Aldrich, St Louis, MO, USA). Images of all of the examined slides were obtained by a Nikon epi-fluorescence microscope system Eclipse 80i; the exposure time and dynamic range of the camera in all of the channels were adjusted to the same values for all of the slides to portray quantitatively comparable images. The images were further processed and merged using NIS-Elements Advanced Research 5.11.03 (instruments and software from Nikon, Tokyo, Japan). Next, each slide was analysed manually for the presence of γH2AX foci and fluorescent foci patterns by visual inspection with the naked eye.

### 2.14. Comet assay

DNA damage was measured using an alkaline version of the comet assay. Cells embedded in 1% agarose (Sigma-Aldrich, St. Louis, MO, USA) on microscope slides were lysed in 10 mM Tris-buffered 2.5 M NaCl (pH 10.0; Penta, Prague, Czech Republic) containing 1% Triton x 100 (Merck Milipore, Billerica, MA, USA) and 100 mM EDTA (Penta, Prague, Czech Republic) for 1 h at 4 °C. The electrophoresis was carried out at 40 V, 300 mA, for 30 min at 4 °C after 40 min of unwinding in alkaline conditions (NaOH, EDTA). DNA damage was analysed by the comet module of Lucia 6.20 image analysis (Laboratory Imaging, Prague, Czech Republic) after the cells were stained with ethidium bromide (Sigma-Aldrich, St. Louis, MO, USA). The percentage of DNA in the comet tail was measured. At least fifty cells per slide were analysed.

### 2.15. ROS-Glo™ Hydrogen peroxide assay

The ROS-Glo™ $H_2O_2$ Assay is a homogeneous, fast and sensitive bioluminescent assay that measures the level of hydrogen peroxide ($H_2O_2$), a reactive oxygen species (ROS), directly in the cell culture or in the defined enzyme reactions. Generation of ROS was detected using the ROS-Glo™ $H_2O_2$ Assay Kit (Promega, Madison, WI, USA) according to the manufacturer's instructions. Briefly, $2 \times 10^4$ were seeded in a 96-well plate, after the 2 or 4 h incubation with 10 and 20 μM of montanine or 50 μM of menadione (positive control $H_2O_2$ inducer), 100 μL of ROS-Glo™ reagent was added to each well. After 20 min of incubation at room temperature, the luminescence was measured using a Tecan Spark multimode microplate reader (Tecan Group, Männedorf, Switzerland).

### 2.16. Western blotting

Whole-cell lysates (Cell Lysis Buffer, Cell Signalling Technology, Danvers, MA, USA) were collected 24 and 72 h following treatment of A549 cells with 2.5 μM and 5 μM of montanine and 4 h following treatment of MOLT-4 cells with 2 μM and 4 μM of montanine. Cells treated with 0.1% DMSO were used as a negative control. Cells treated with 5 μM of cisplatin or 0.25 μM of doxorubicin were used as positive controls. Quantification of the protein content was determined using the BCA assay (Sigma-Aldrich, St. Louis, MO, USA). The lysates (20 μg of purified protein) were loaded into lanes of polyacrylamide gel and were subjected to electrophoresis. After electrophoresis separation, the proteins were transferred to a PVDF membrane (Bio-Rad, Hercules, CA, USA). Any non-specific bindings of the membranes were blocked for 1 h in a Tris-buffered saline (TBS) containing 0.05% Tween 20% and 5%, w/v, non-fat dry milk. The membranes were washed in TBS. Incubation with a primary antibody against specific antigens Cdc25A, Chk1, Chk1_serine 345, ERK, ERK ½_threonine 202 and tyrosine 204, p21, p27, Akt, Akt_threonine 308, p38, p38_ threonine 180 and tyrosine 182, Bax from Cell Signalling Technology (Danvers, MA, USA) and β-actin from Sigma-Aldrich (St. Louis, MO, USA) was performed at 4 °C overnight. The following day the membranes were washed 5-times with TBS, each time for 5 min, and once with TBS for 10 min, and then incubated with an appropriate secondary antibody (DakoCytomation, Glostrup, Denmark or Cell Signalling Technology, Danvers, MA, USA) for 1 h at room temperature. Band detection was performed using a chemiluminescence detection kit (Roche, Basel, Switzerland). To ensure equal protein loading, each membrane was reprobed and β-actin was detected. The densities of the proteins of interest were analysed using the GeneTools image analysis system (Syngene, Cambridge, UK).

### 2.17. Data and statistical analysis

The descriptive statistics of the results were calculated, and the charts were made using either Microsoft Office 365 Excel (Microsoft, Redmond, WA, USA) or GraphPad Prism 7 biostatistics (GraphPad Software, La Jolla, CA, USA) software. In this study, all the values were expressed as arithmetic means with SD of triplicates, unless otherwise noted. For quantitative data, normality testing was performed to assess whether parametric or nonparametric tests should be used. For

experiments with parametric variables, the significant differences between the groups were analysed using the unpaired Student's *t*-test. The level of significance is indicated as * $p < 0.05$, * * $p < 0.01$, * ** $p < 0.001$. $IC_{50}$ values were calculated based on data obtained from proliferation determined by a WST-1 assay and processed using GraphPad Prism 7 biostatistics (GraphPad Software, San Diego, CA, USA) software. Drug concentrations were plotted against the percentage of cell proliferation/viability and the $IC_{50}$ values were determined using nonlinear regression. The statistics for comet assay results were calculated using NCSS software (NCSS, Kaysville, UT, USA). Differences within the groups were evaluated using a nonparametric Kruskal-Wallis one-way analysis of variance, followed by Dunn's post-hoc test with Bonferoni's correction. All experimental data were expressed as median and 25th and 75th percentiles.

## 3. Results

### 3.1. Preparation of montanine derivatives (1–15)

A previously described procedure was used to obtain the corresponding esters **1**–**15** [23], and montanine was isolated from *Hippeastrum x hybridum* cv. Ferrari, as reported by our research group [25]. The

**Table 1**
Antiproliferative activity of montanine derivatives, manthine and montanine. Cells were treated with a 10 μM concentration for 48 h, and their proliferation was quantified using a WST-1 assay and expressed as the percentage of control cells (0.1% DMSO treated, proliferation 100%). Each value represents the mean of experiments that were repeated independently for a minimum of three times. Values from the intervals 0–25%, 26–50% and 51–75% of viable cells are highlighted using different colors. Doxorubicin at 1 μM was used as a reference drug. Mock treatment by 0.1% DMSO was used as a negative control.

| | Jurkat | MOLT-4 | A549 | HT-29 | PANC-1 | A2780 | MCF-7 | SAOS-2 | MRC-5 |
|---|---|---|---|---|---|---|---|---|---|
| **1** | 105 | 84 | 89 | 67 | 109 | 137 | 80 | 97 | 101 |
| **2** | 85 | 84 | 87 | 72 | 104 | 99 | 80 | 96 | 90 |
| **3** | 44 | 36 | 55 | 62 | 69 | 77 | 54 | 46 | 60 |
| **4** | 55 | 44 | 66 | 52 | 87 | 95 | 54 | 54 | 72 |
| **5** | 91 | 88 | 91 | 89 | 114 | 108 | 80 | 92 | 102 |
| **6** | 100 | 84 | 81 | 89 | 100 | 93 | 78 | 94 | 96 |
| **7** | 87 | 93 | 99 | 93 | 94 | 99 | 69 | 86 | 104 |
| **8** | 86 | 75 | 78 | 67 | 93 | 120 | 77 | 76 | 85 |
| **9** | 92 | 94 | 81 | 66 | 98 | 113 | 76 | 89 | 89 |
| **10** | 119 | 82 | 86 | 82 | 95 | 107 | 77 | 90 | 96 |
| **11** | 71 | 47 | 78 | 79 | 81 | 92 | 56 | 70 | 82 |
| **12** | 8 | 3 | 28 | 38 | 39 | 39 | 19 | 25 | 35 |
| **13** | 67 | 52 | 64 | 88 | 63 | 87 | 36 | 51 | 64 |
| **14** | 1 | 1 | 6 | 4 | 26 | 12 | 8 | 1 | 2 |
| **15** | 47 | 28 | 70 | 65 | 57 | 67 | 21 | 36 | 47 |
| **Manthine** | 15 | 5 | 29 | 44 | 41 | 47 | 14 | 34 | 29 |
| **Montanine** | 4 | 2 | 23 | 36 | 29 | 26 | 12 | 25 | 22 |
| **DOX** | 2 | 1 | 12 | 36 | 60 | 10 | 31 | 13 | 43 |

| |
|---|
| 0-25% |
| 26-50% |
| 51-75% |

synthesis of derivatives **1**–**12** is shown in Fig. 1, and compounds **13**–**15** were synthesised as described previously in the literature [23]. Manthine was prepared according to a published procedure [22] via the intramolecular rearrangement of haemanthamine, which was previously isolated from *Zephyranthes citrina* Baker [26].

### 3.2. Montanine, 12, 14, and manthine display the most potent cytotoxicity

The potential of manthine, montanine and the montanine derivatives (**1**–**15**) to suppress the proliferation and viability of different histological types of cancer cell lines (leukemia – Jurkat, MOLT-4; lung adenocarcinoma – A549; colorectal adenocarcinoma – HT-29; pancreas carcinoma – PANC-1; ovarian carcinoma – A2780; breast adenocarcinoma – MCF-7; osteosarcoma – SAOS-2) and one non-cancer cell line (fetal lung fibroblasts – MRC-5) was assessed using the metabolic activity assay WST-1 at 48 h post treatment with a single dose at 10 μM. In the next step, the growth percentage (GP) value of each alkaloid compound was determined, and a GP value < 50% (at least 50% tumour growth inhibition) was established as the threshold for valuable cytotoxic molecules in an $IC_{50}$ value range below 10 μM. As shown in Table 1 and Fig. 2, the inhibitory rates indicated that montanine, **12**, **14** and manthine showed high cytotoxicity at this initial concentration (10 μM), as the GP (%) values were lower than the < 50% threshold value considered for inhibitory compounds. The GP values of the resultant compounds, montanine, **12**, **14** and manthine were below 50% for all determined cell lines, and they were further investigated by determining the corresponding 50% inhibitory concentration $IC_{50}$ values (Table 2). Compounds **12**, **14** and manthine exhibited surprising cytotoxic

**Table 2**
$IC_{50}$ values of montanine derivatives 12 and 14, manthine and montanine in human cancer and non-cancer cells[a,b].

| Cell type | 12 | 14 | Manthine | Montanine [21] |
|---|---|---|---|---|
| **Jurkat** | 2.58 ± 1.07 | 3.40 ± 1.04 | 3.02 ± 1.05 | 1.04 ± 0.14 |
| **MOLT-4** | 2.95 ± 1.08 | 1.56 ± 1.09 | 3.51 ± 1.20 | 1.26 ± 0.11 |
| **A549** | 1.55 ± 1.19 | 1.41 ± 1.09 | 6.18 ± 1.15 | 1.09 ± 0.31 |
| **HT-29** | 2.16 ± 1.17 | 2.11 ± 1.05 | 19.69 ± 1.19 | 1.35 ± 0.47 |
| **PANC-1** | 1.88 ± 1.11 | 8.02 ± 1.06 | 7.69 ± 1.18 | 2.30 ± 0.45 |
| **A2780** | 2.70 ± 1.14 | 8.06 ± 1.06 | 12.94 ± 1.16 | 1.67 ± 0.29 |
| **MCF-7** | 1.65 ± 1.12 | 1.89 ± 1.07 | 2.68 ± 1.08 | 1.39 ± 0.21 |
| **SAOS-2** | 1.18 ± 1.17 | 2.13 ± 1.06 | 4.06 ± 1.13 | 1.36 ± 0.49 |
| **MRC-5** | 2.18 ± 1.17 | 1.54 ± 1.06 | 3.60 ± 1.14 | 1.79 ± 0.50 |

[a] Results are expressed in μM.
[b] Results are the mean values ± SD of experiments that were repeated independently for a minimum of three times.

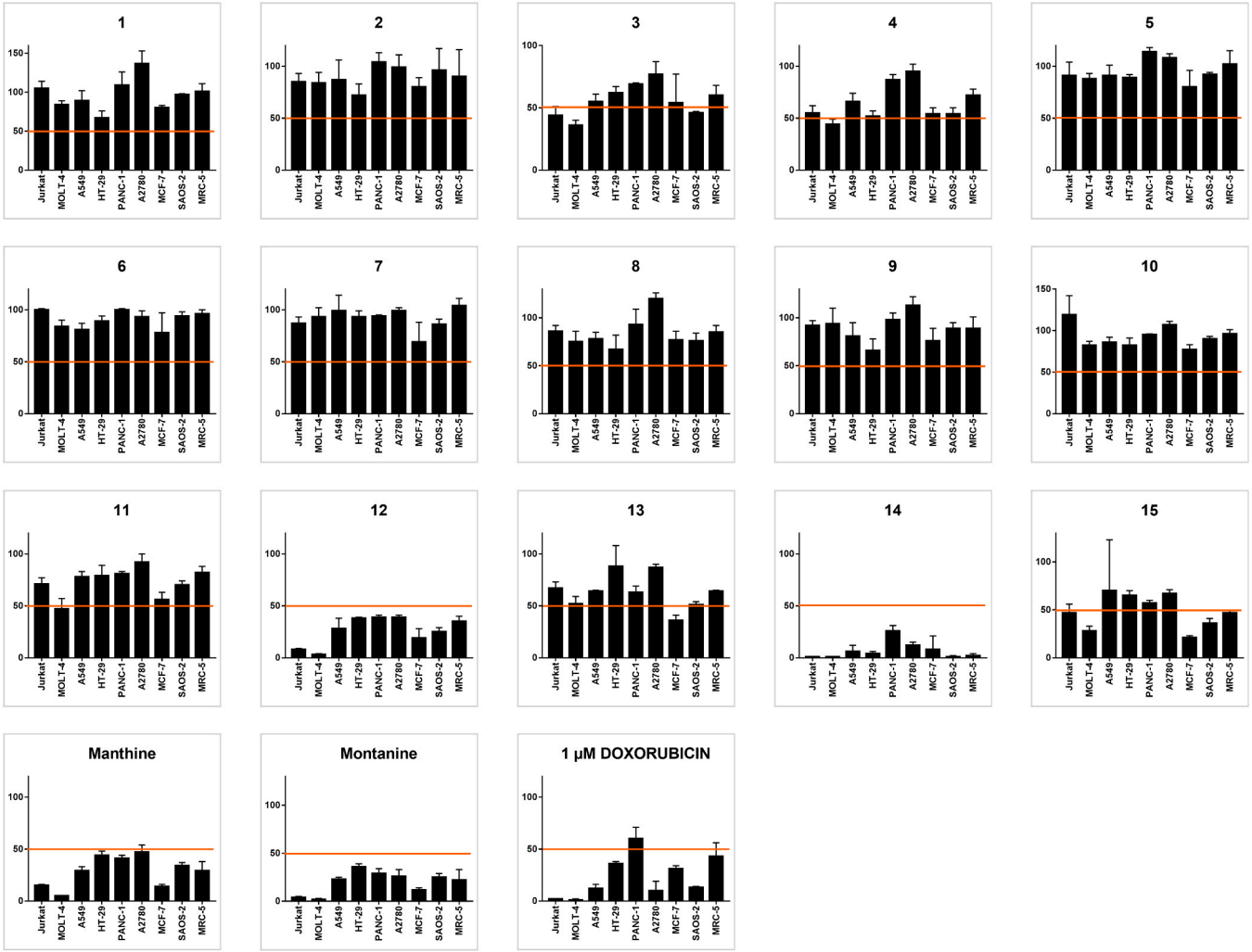


**Fig. 2.** Antiproliferative activity of all tested compounds (**1**–**15**, manthine, montanine, positive control doxorubicin). Each graph represents one compound and its effect on the proliferation of 9 cell lines. Cells were treated with a concentration of 10 μM for 48 h, and their proliferation was established using a WST-1 assay and expressed as the percentage of control cells (0.1% DMSO treated, proliferation 100%). Each value represents the mean ± standard deviation of experiments that were repeated independently for a minimum of three times. The horizontal orange line borders the 50% value. Doxorubicin was tested at 1 μM.

properties at low micromolar $IC_{50}$ concentrations. The $IC_{50}$ values of derivative **12** ranged from 1.18 μM to 2.95 μM, and those of derivative **14** ranged from 1.41 μM to 8.06 μM. Manthine exerted varying and moderate degrees of cytotoxicity, with $IC_{50}$ values ranging from 2.68 μM to 19.69 μM. Remarkably, parent montanine, which had been tested in our previous study [21] exhibited distinctively lower $IC_{50}$ values ranging from $IC_{50}$ 1.04 μM to 2.30 μM. Collectively, the decreasing order of the mean $IC_{50}$ values for these compounds was as follows: manthine (< 8 μM), **14** (< 4 μM), **12** (< 3 μM) and montanine (< 2 μM). Therefore, montanine was selected for the subsequent assays because it displayed the most pronounced activity.

### 3.3. Montanine inhibits the proliferation of selected solid cancer lines

Montanine was identified as the isoquinoline alkaloid with the greatest inhibitory activity at $IC_{50}$ (range of 1.04–2.30 μM); therefore, the effects on cancer cell growth and survival were cross-verified at varying concentrations. According to the results obtained using the endpoint method based on the principle of the reduction of tetrazolium salt WST-1, the real-time label-free cell proliferation system xCELLigence RTCA was used to dynamically monitor the long-term treatment effect of montanine on cancer cells spanning four types of solid tumours. The xCELLigence system was designed to conduct a dynamic analysis of cell adhesion, morphology, viability, and the number of cells based on

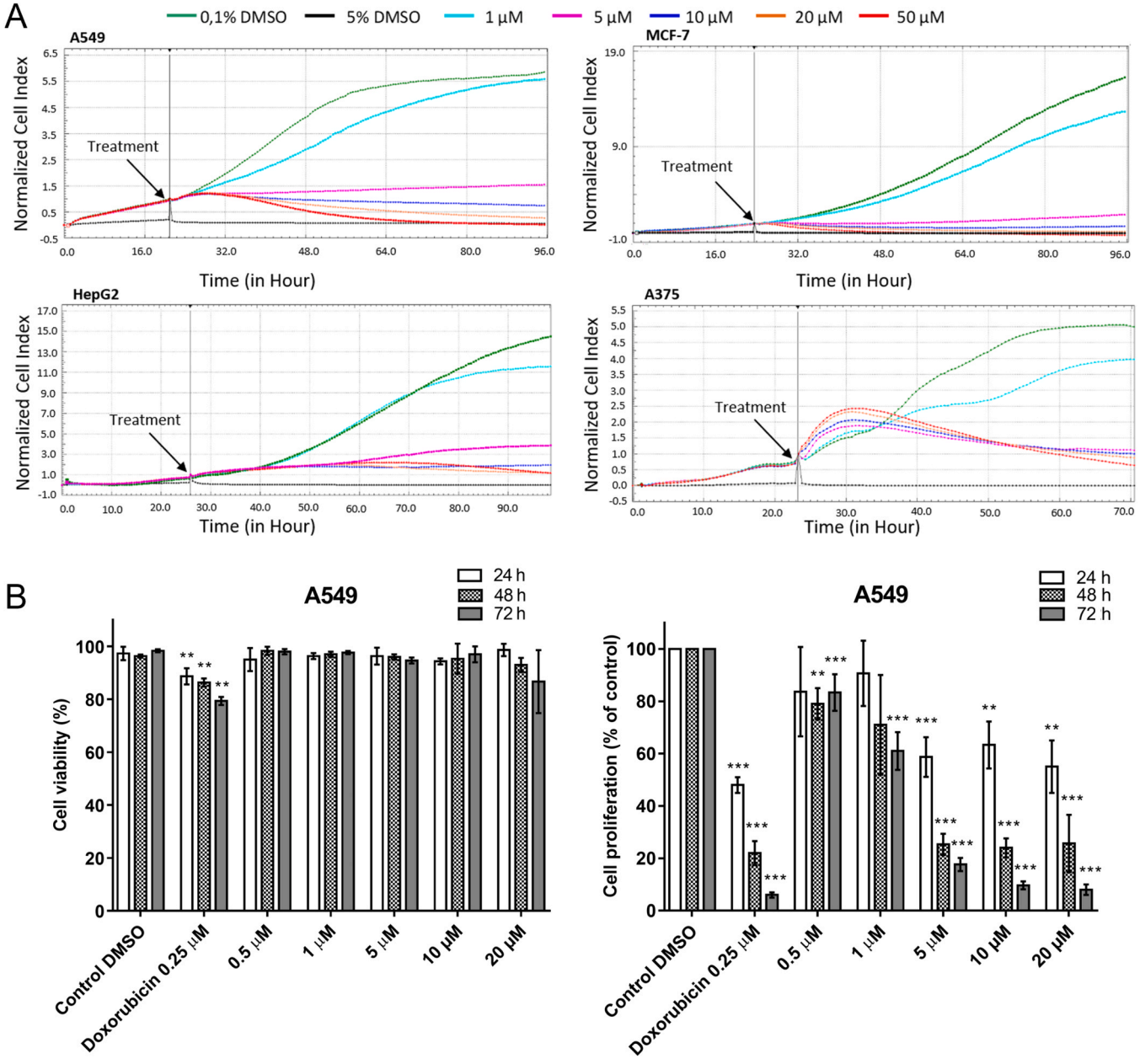


**Fig. 3.** Cell proliferation and cytotoxicity of montanine in human cancer cells of various tumour histotypes. (A) A549, MCF-7, HepG2, and A375 cells were treated with montanine at concentrations ranging from 0 μM to 50 μM for 72 h. Cell proliferation was measured with the xCELLigence RTCA electrical impedance system. Cells treated with 0.1% DMSO were used as the vehicle control and 5% DMSO-treated cells as the positive control. Plots shown are representative of at least three replicate experiments in each case. (B) Cell viability and proliferation of A549 cells were determined at 24 h, 48 h and 72 h after treatment with different doses of montanine (0.5 μM, 1 μM, 5 μM, 10 μM and 20 μM) using the Trypan blue exclusion test. Error bars represent SD. The test was conducted in triplicate (n = 3) as described in the Materials and Methods. * $p < 0.05$, * * $p < 0.01$ and * ** $p < 0.001$, *t*-test. Cells treated with 0.25 μM doxorubicin and 0.1% DMSO were used as the positive and negative control, respectively.

impedance, which are displayed as normalised cell index (CI) values. This continuous method used to monitor cellular responses after treatment does not require exogenous labels. The effect on proliferation was observed in lung adenocarcinoma A549, breast adenocarcinoma MCF-7, hepatocellular carcinoma HepG2 and malignant melanoma A375 cells using montanine concentrations of 1 μM, 5 μM, 10 μM, 20 μM and 50 μM dosed approximately 24 h after cell seeding, where the cells were in logarithmic growth and followed up for 72 h of incubation. Cells treated with 0.1% of DMSO were used as vehicle controls and cells treated with 5% of DMSO as a positive controls. As shown in Fig. 3**A,** real-time cell proliferation curves clearly demonstrate the concentration-dependent growth inhibitory activity of montanine in all tested cancer cells. Montanine at 1 μM exhibited delayed cell proliferation compared to 0.1% DMSO, and cells treated with 5 μM showed signs of recovery in the late periods of proliferation profiles. Furthermore, at higher doses (10, 20, and 50 μM), the inhibitory effect of montanine becomes even stronger with increasing treatment time.

To assess whether montanine treatment could promote alterations in cell viability and proliferation, a Trypan blue dye exclusion assay was performed. The percentage of viable cells and the percentage change in cell proliferation (i.e., cell number) with respect to the negative control were quantified 24 h, 48 h and 72 h after treatment with montanine concentrations of 0.5 μM, 1 μM, 5 μM, 10 μM and 20 μM. As shown in Fig. 3**B**, the results indicated the significant cytostatic activity of montanine against the A549 cell line, even when using the lowest concentration of 0.5 μM dosed for 48 h ($p < 0.01$) and 72 h ($p < 0.001$). With an increasing montanine concentration, a greater decrease in cell growth was observed. Moreover, the longer the incubation of A549 cells with montanine, the more pronounced the reduction in cell proliferation. Furthermore, montanine showed no significant cytotoxicity, even after exposure to the highest dose of 20 μM over the investigated period of 72 h.

### *3.4. Montanine suppresses the growth of lung adenocarcinoma A549 by activating the cell cycle checkpoints and the redistribution of cell cycle*

The Trypan blue exclusion test showed that montanine had the greatest potential to inhibit cancer cell proliferation. Therefore, flow cytometry was used to detect the effect of montanine on the percentage of A549 cells in different phases of the cell cycle after 24 h and 72 h of treatment. As revealed in Fig. 4**A**, a significant ($p < 0.01$) redistribution of cell cycle was observed starting from 5 μM of montanine and 24 h of treatment. When the cells were treated with 5 μM for 24 h, a large reduction in the number of S-phase cells was observed, indicating lower proliferation. Conversely, the strong significant decrease in A549 cells in the G1 phase was detected using 20 μM ($p < 0.01$) and 40 μM ($p < 0.001$) of treatment. As shown in Fig. 4**B**, prolonged 72-h treatment with montanine at low concentrations (0.5 μM, 1 μM and 5 μM) increased the percentage of cells in the G1 phase, and a consequent decrease in the percentage of cells in the S and G2 phases was observed. Compared to the 0.1% DMSO solvent control, montanine treatment at higher doses (10 μM and 20 μM) resulted in the accumulation of A549 cells mainly in the G2 phase: the proportion of cells in the G2 phase increased considerably from 16% (control cells) to 23% (10 μM) and 25% (20 μM), respectively. As no significant effect of montanine on A549 cell viability was observed over the entire concentration range tested (0.5–20 μM), we subsequently validated the lack of apoptosis activation by measuring caspase-3, − 7, − 8 and − 9 activity after 24 h of exposure. As depicted in Fig. 4**C**, montanine did not significantly affect the induction of apoptotic cell death in A549 cells via the activation of the main executor caspases (caspase −3 and −7) of apoptosis, caspase − 8 responsible for extrinsic apoptotic pathway, or caspase − 9 responding to internally induced apoptotic pathway. Since the decrease in cell proliferation and cell cycle redistribution after montanine treatment were considered closely correlated, the proteins involved in this effect, specifically M-phase inducer phosphatase I (cdc25A), extracellular regulated kinase 1/2 (ERK1/2), p38 mitogen-activated protein kinase (MAPK), Akt protein kinase and cyclin-dependent protein kinase inhibitor p27 were evaluated using electrophoresis and Western blotting at 24 h and 72 h post-treatment. Fig. 4**D** shows the change in G1 phase cell cycle arrest-related protein levels at 24 h and 72 h after application of montanine at 2.5 μM and 5 μM. Decreases in cdc25A phosphatase levels with a concomitant increase in p27 protein levels and a consequent decrease in Akt kinase phosphorylated at Thr308 were observed using 2.5 μM and 5 μM concentrations at 72 h. With respect to the activation of p38 MAPK, hyperphosphorylation at Thr180 and Tyr182 occurred after 24 h and 72 h from the application of montanine, and ERK phosphorylated at Thr202 and Tyr204 was downregulated in the same time interval. Summary bar graphs showing relative protein levels normalized against β-actin or protein levels in its unphosphorylated form are depicted in the Supplementary material (Fig. S1).

### *3.5. Montanine suppresses the growth of leukemic MOLT-4 cells, significantly decreases the viability of MOLT-4 cells and leads to cell cycle arrest*

The results of initial single-dose screening (where montanine exhibited a percentage growth value 2%) showed that the MOLT-4 T-lymphoblastic leukemia cell line was among the most sensitive cell lines affected by treatment. Therefore, the effects of alkaloid treatment on MOLT-4 cells viability and proliferation were determined using the Trypan blue exclusion test. Fig. 5**A** shows the effect of montanine on the viability and proliferation of leukemia cells. A significant ($p < 0.01$) effect on the viability of MOLT-4 cells was observed using a concentration of 1 μM and a 48 h interval, and montanine at a higher concentration of 2 μM decreased ($p < 0.05$) the number of viable leukemic cells over a 24 h spell. The strongest ($p < 0.001$) impact on the viability of leukemic cells treated with 5 μM montanine for 48 h, where approximately 50% of the MOLT-4 cells were not viable compared to the negative control. According to the determination of MOLT-4 cells growth inhibition depicted in Fig. 5**A**, a significant decrease in proliferation was observed after using the lowest montanine concentration of 1 μM ($p < 0.01$) and 48 h of treatment. At a 24 h time interval, a significant ($p < 0.05$) reduction in proliferation was apparent when using 2 μM of montanine. The same concentration applied for 48 h suppressed the proliferation of MOLT-4 even more significantly ($p < 0.001$), and this effect became even more pronounced over time. Notably, with increasing montanine concentrations, the proliferation of MOLT-4 cells decreased considerably at both time points.

Based on the Trypan blue assay results, in which cell growth was inhibited, we investigated the cell cycle distribution by flow cytometry (Fig. 5**B**). To detect the impact of montanine on the cell cycle, MOLT-4 cells were treated with montanine concentrations of 1 μM, 2 μM and 3 μM for 24 h. Significant alterations in the cell cycle population were observed even at the lowest montanine concentration. Exposure to 1 μM of montanine caused a significant ($p < 0.001$) increase in the number of cells in the G1 phase, which was concomitant with a significant ($p < 0.01$) decrease in the cell population within the S phase of the cell cycle. Congruently, a higher montanine concentration of 2 μM resulted in a similar trend: a considerable ($p < 0.001$) increase in the number of cells in the G1 phase and a reduction in the number of cells in the S phase compared to the number of control cells. Furthermore, montanine applied at the highest dose of 3 μM had a significant ($p < 0.01$) impact on the G2 phase, with an increase in the cell population in the G2 phase compared to the negative control.

To further elucidate the functional effects of montanine on the cell cycle, we detected proteins involved in the redistribution of cells in different cell cycle phases. To examine whether treatment affected the levels of cell cycle-related proteins, the expression and/or activation of target proteins was determined by Western blot 4 h after treatment with montanine at 2 μM and 4 μM. As shown in Fig. 5**C**, montanine at 2 μM

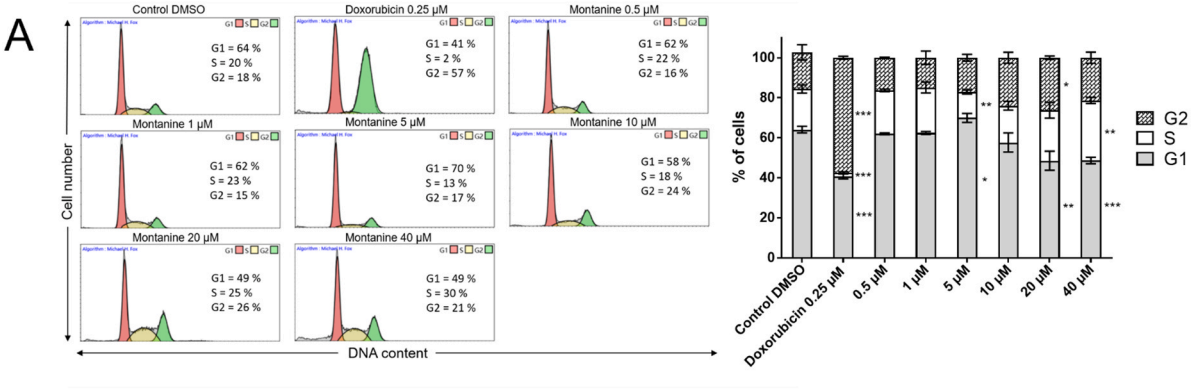


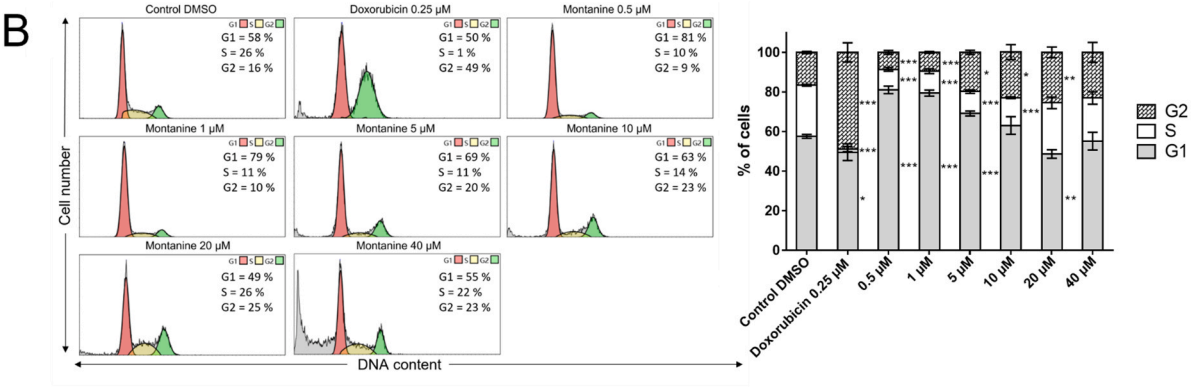


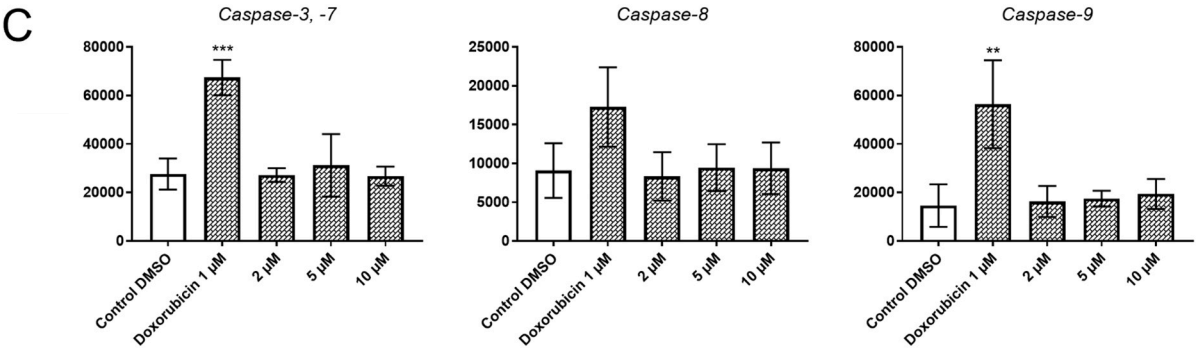


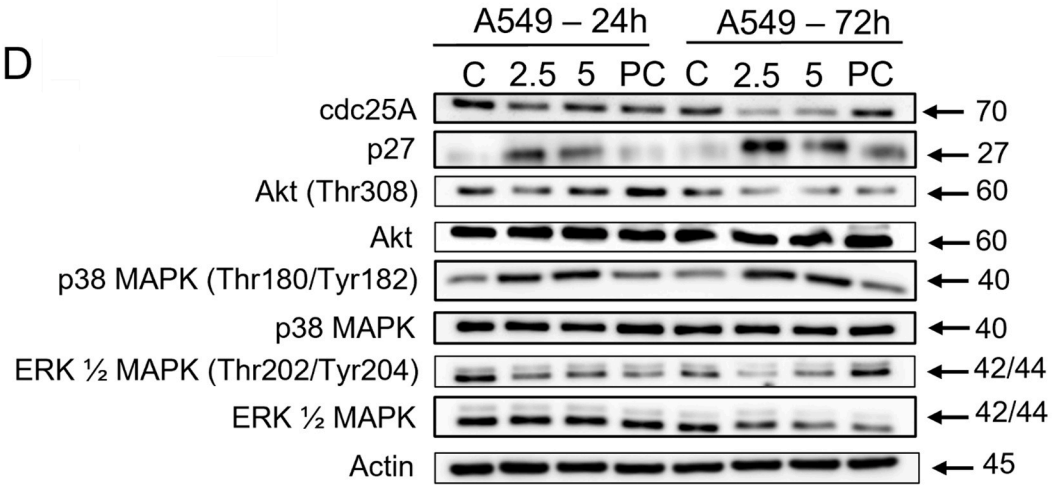


(caption on next page)

**Fig. 4.** Montanine induced changed cell cycle distribution but not apoptosis of A549 cells. A549 cells were incubated with increasing concentrations of montanine (0.5 μM, 1 μM, 5 μM, 10 μM, 20 μM and 40 μM) for 24 h (A) and 72 h (B) respectively, and then analysed using flow cytometry. Representative histograms (with mean percentage of cells cycling through phases G1, S, and G2) and bar graphs (summarising percentage number of cells in each phase of the cell cycle) are displayed. (C) The effect of montanine on caspase-3, caspase-7, caspase-8, and caspase-9 activities in A549 cells treated with montanine at 2 μM, 5 μM or 10 μM for 24 h. Results show mean values ± SD of experiments that were repeated independently for a minimum of three times. * $p < 0.05$, * * $p < 0.01$ and * ** $p < 0.001$, *t*-test. (D) Western blotting was used to detect the effect of montanine on the expression and activation of cell cycle-related proteins in A549 cancer cells after exposure to 2.5 μM or 5 μM montanine for 24 h and 72 h. C, negative control; PC, positive control; 2.5, montanine at 2.5 μM; 5, montanine at 5 μM. Cells treated with 0.25 μM (cell cycle and Western blot analysis) or 1 μM (quantification of caspases activity) doxorubicin and 0.1% DMSO were used as the positive and negative control, respectively.

and 4 μM induced the phosphorylation of Chk1 at Ser345. This kinase coordinates the cell cycle checkpoint in the G1/S phase, and it was also associated with upregulation of the p21 protein after montanine administration at both concentrations. We then investigated whether montanine caused the loss of MOLT-4 cell viability through an apoptotic mechanism. Pro-apoptotic activity was supported by the upregulation of Bax protein after montanine treatment at 2 μM and 4 μM. Among the MAP kinases that marked the occurrence of cell cycle arrest and apoptosis, p38 MAPK activation was determined in the MOLT-4 cell line. Montanine treatment activated p38 MAPK through phosphorylation of Thr180 and Tyr182. Summary bar graphs showing relative protein levels normalized against β-actin or protein levels in its unphosphorylated form are depicted in the Supplementary material (Fig. S2).

### 3.6. Decrease in the viability of MOLT-4 cells is related to apoptotic cell death

As montanine treatment upregulated the pro-apoptotic protein Bax, we conducted apoptotic experiments to confirm cell death elicited by isoquinoline treatment and to quantify the apoptotic cell populations. The apoptotic cell death of MOLT-4 cells was evidenced by the measuring the activity of caspase − 3, − 7, − 8 and − 9; early and late apoptotic cells were quantified using Annexin V/PI staining; and the mitochondrial membrane potential was assessed. The results in Fig. 6**A** demonstrate that the activity of effector caspase − 3 and − 7 was significantly increased after using 2 μM ($p < 0.01$), 5 μM ($p < 0.001$) and 10 μM ($p < 0.001$) montanine applied for 24 h. Moreover, incubating cells for 24-h at montanine concentrations of 2 μM, 5 μM and 10 μM significantly activated apical caspases of intrinsic apoptotic pathways ($p < 0.05$), and those of extrinsic apoptotic pathways were significantly activated ($p < 0.05$) at the highest concentration (10 μM).

To further investigate whether the inhibitory effect of montanine was associated with cell apoptosis, an Annexin V Alexa Fluor®488 /PI binding assay was conducted. As illustrated in Fig. 6**B**, 24 h after treatment with montanine at concentrations of 1 μM, 2 μM, 3 μM, 4 μM and 5 μM, the percentage of cells in the early phase of apoptosis was 2%, 6%, 14%, 22% and 22%, respectively, and the percentage of cells in the late phase of apoptosis was 8%, 14%, 19%, 24%, and 28% respectively. The apoptotic status was increased by the sum of cells in the early and late phases of apoptosis, and they were significantly activated following exposure to montanine at 2 μM, 3 μM, 4 μM and 5 μM ($p < 0.001$).

To investigate whether apoptosis in MOLT-4 cells induced by montanine was executed by the collapse of mitochondrial membrane potential (Δψm), we examined this by flow cytometry using mitochondrial probe JC-1. As shown in Fig. 6**C**, culturing MOLT-4 cells with 1 μM montanine for 24 h caused significant ($p < 0.05$) depolarisation of the mitochondrial membrane. After montanine treatment at 2 μM, the population of cells containing depolarised mitochondria increased considerably to 33% ($p < 0.001$), and the population tended to increase with increasing doses.

### 3.7. Montanine induces single-strand DNA damage, but has no effect on double-strand DNA breaks and ROS formation in MOLT-4 cells

To further investigate the montanine-related pro-apoptotic activity in MOLT-4 cells, three crucial genotoxic stress markers (single-strand DNA (ssDNA) break induction, intracellular ROS level and γH2AX formation) were explored. Certain plant-derived chemotherapeutic agents are known to exert anticancer effects via DNA damage, leading to apoptotic cell death [27]. An alkaline comet assay was therefore performed to determine whether montanine induces DNA damage. As depicted in Fig. 7**A**, the ssDNA breaks were significantly ($p < 0.05$) increased at an early time point (2 h) after starting montanine treatment at a concentration of 5 μM. A higher dose of montanine (10 μM) introduced considerable ssDNA breaks after 2 h ($p < 0.001$) and 4 h ($p < 0.001$) and persisted at high levels beyond 12 h ($p < 0.05$). ROS generation is associated with DNA damage, mitochondrial depolarisation, and apoptosis; therefore, we examined ROS formation (Fig. 7**B**). Compared to the well-known ROS inducer menadione, montanine did not lead to increased levels of intracellular ROS in a time- (2 h and 4 h) or concentration-dependent manner (5 μM and 10 μM). The phosphorylation of histone H2AX at serine 139 (γH2AX) is the first step in the recruitment and localisation of DNA repair proteins at sites of DNA double-strand breaks following DNA damage. Immunofluorescence staining of γH2AX, and epifluorescence microscopy were performed to determine whether montanine exposure caused dsDNA breaks (Fig. 7**C**). Exposure to montanine at concentrations of 5 μM and 10 μM for 2 h did not lead to a significant increase in γH2AX foci formation. In addition, the cells of the positive control group treated with the dsDNA break inducer doxorubicin at 0.1 μM displayed increased levels of red γH2AX protein foci throughout the nucleus.

## 4. Discussion

There has been increasing interest in the search for novel chemotherapeutic agents against cancer, which has prompted researchers to identify innovative sources of anticancer compounds from plant secondary metabolites. Our group previously reported the isolation of the alkaloid montanine from *Hippeastrum* cultivars, which exerts a potent antiproliferative effect against tumour cell lines of various histotypes [21]. We demonstrated that montanine inhibits the growth of cancer cells with $IC_{50}$ values in the concentration range from 1.04 μM to 2.30 μM, and this was determined for different tumour types, including drug-insensitive cell lines such as non-small cell lung cancer (NSCLC) A549 or pancreatic adenocarcinoma PANC-1 [28]. In another study, investigating the cytotoxic effects of alkaloids from *Haemanthus humilis*, the cytotoxicity of montanine against breast (MCF7, Hs578T, MDA-MB-231), colon (HCT-15), lung (A549) and melanoma (SK-MEL-28) cells was found in the range of 1.9 μM to 23.2 μM [20]. Comparing the related study of Masi et al. with our work, we confirmed that montanine isolated from *Hippeastrum* cultivars shows similar inhibitory activity against cancer cell lines [21]. These findings, as well as the presence of a unique 5,11-methanomorphanthridine skeleton, have sparked the interest of researchers in developing semisynthetic candidates with the potential to enhance the inhibitory activity, investigate the effect of the introduction of aromatic groups and gain more knowledge about the mechanism of action of montanine-type isoquinoline alkaloids.

Previous studies have revealed that the skeletal rearrangement of the alkaloid haemanthamine may be used to generate compounds with an alkaloid montanine ring system [22,29]. Among the parent haemanthamine and montanine analogues prepared by the semisynthetic

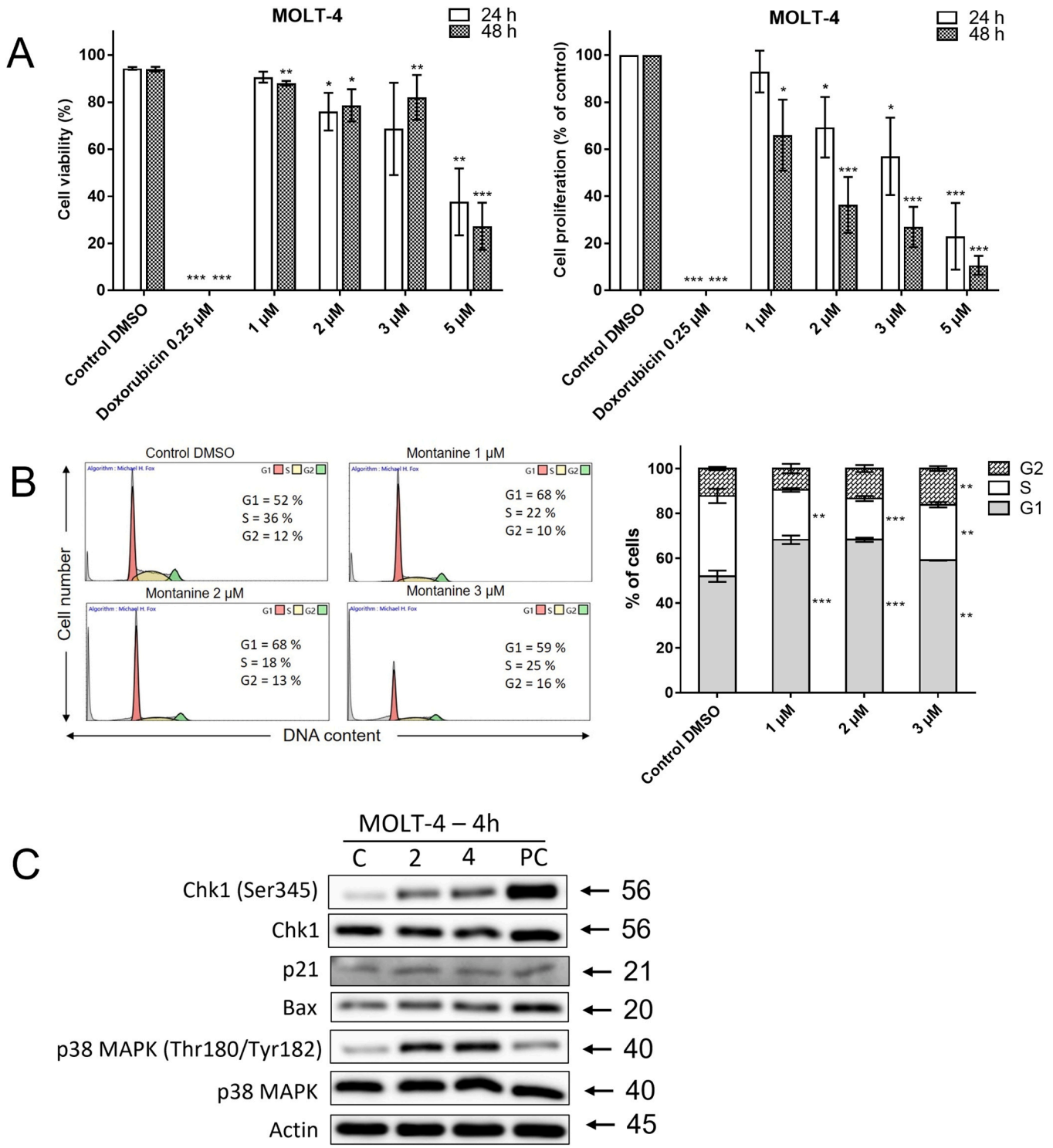


**Fig. 5.** Effect of montanine on cell viability, proliferation and cell cycle progression in MOLT-4 and cells. (A) Human acute lymphoblastic leukemia MOLT-4 cells were treated with different concentrations (1 µM, 2 µM, 3 µM and 5 µM) of montanine for 24 h and 48 h, respectively. Cell viability and proliferation were examined by Trypan blue dye exclusion staining. (B) Effect of montanine on cell cycle progression. MOLT-4 cells were exposed to montanine at increasing doses for 24 h, and the cells were then stained with PI and their DNA content was analysed by flow cytometry. Representative histograms (with mean percentage of cells cycling through phases G1, S and G2) and bar graphs (summarising percentage of cells in each phase of the cell cycle) are displayed. (C) Cell cycle regulatory and cell apoptotic proteins were detected by Western blot after montanine treatment at 2 µM and 4 µM for 4 h. C, negative control; PC, positive control; 2, montanine at 2 µM; 4, montanine at 4 µM. Cells treated with 0.25 µM doxorubicin (viability and proliferation assay) or 5 µM cisplatin (Western blot analysis) and 0.1% DMSO were used as the positive and negative control, respectively. All quantitative data are expressed as the mean ± SD from three determinations per condition. * $p < 0.05$, * * $p < 0.01$ and * ** $p < 0.001$, *t*-test.

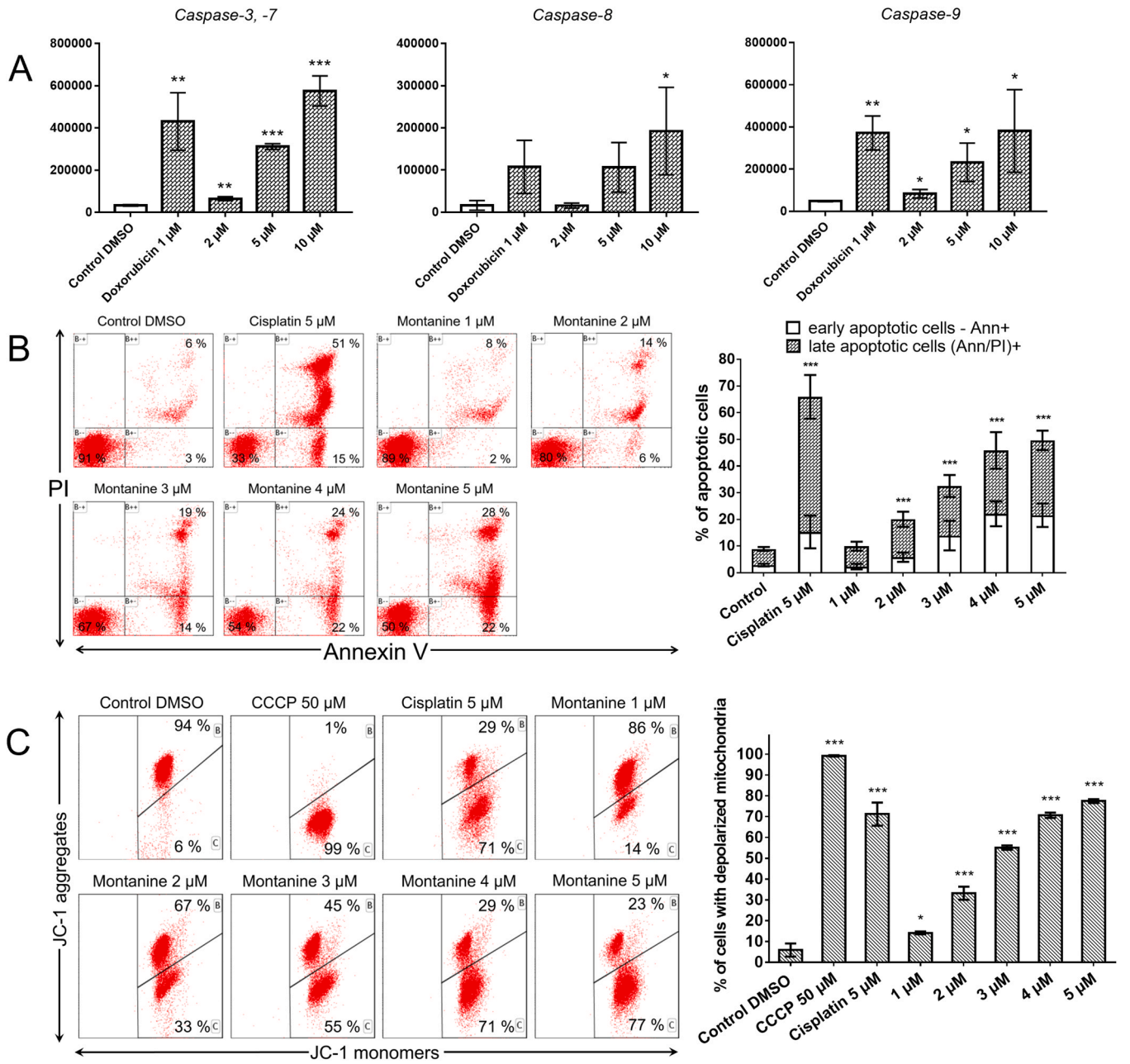


**Fig. 6.** Induction of apoptosis by montanine in MOLT-4 cells. (A) Effects of montanine on the activation of caspase-3, caspase-7, caspase-8 and caspase-9 at concentrations 2 µM, 5 µM and 10 µM in 24 h-treated MOLT-4 cells. Results are expressed as mean ± SD of experiments that were repeated independently for a minimum of three times. Cells treated with 1 µM doxorubicin and 0.1% DMSO were used as the positive and negative control, respectively. MOLT-4 cells were incubated with montanine concentrations of 1 µM, 2 µM, 3 µM, 4 µM and 5 µM for 24 h and then analysed by flow cytometry. (B) Apoptosis was examined with Annexin V/PI staining. Representative histogram showing one of experiment that were repeated independently for a minimum of three times and bar graph showing percentages of early and late apoptotic cells. Cells treated with 5 µM cisplatin and 0.1% DMSO were used as the positive and negative control, respectively. (C) Flow cytometric assessment of mitochondrial membrane potential (Δψm) in MOLT-4 cells exposed to the indicated concentrations of montanine. Representative flow cytometry histograms showing the percentages of cells with high Δψm (containing polarised mitochondria) and low Δψm (containing depolarised mitochondria). Cells treated with 50 µM carbonyl cyanide 3-chlorophenylhydrazone (a protonophore agent) and 5 µM cisplatin were used as the positive control for determining the decreased mitochondrial membrane potential. The bar graph displays the mean ± SD of experiments that were repeated independently for a minimum of three times. * $p < 0.05$, * * $p < 0.01$ and * ** $p < 0.001$, *t*-test.

transformation of haemanthamine, manthine and an indole-containing C2-substituent in ring E of 5,11-methanomorphanthridine and haemanthamine significantly reduced proliferation at concentrations as low as 1 µM [22]. Accordingly, as part of our ongoing research, modifications to the stereocentre at C3 within the E ring resulted in a collection of different montanine derivatives that were screened for their cytostatic and cytotoxic activities. Among the prepared montanine derivatives, only compound **12** with a 3-*O*-(3,5-dinitrobenzoyl) substitution at C3, **14** with a 3-*O*-(4-chloro-3-nitrobenzoyl) substitution at C3 and manthine displayed the most potent cytostatic activity. Moreover, consistent with the study of Govindaraju et al., 2018 [22], we found that manthine exhibited an $IC_{50}$ value in the range of 2.68 −19.69 µM in selected cancer cells.

Considering that montanine is one of the most effective alkaloids in Amaryllidaceae [19–21], and its mean $IC_{50}$ value was lower than that of manthine and the other derivatives, we selected montanine for further

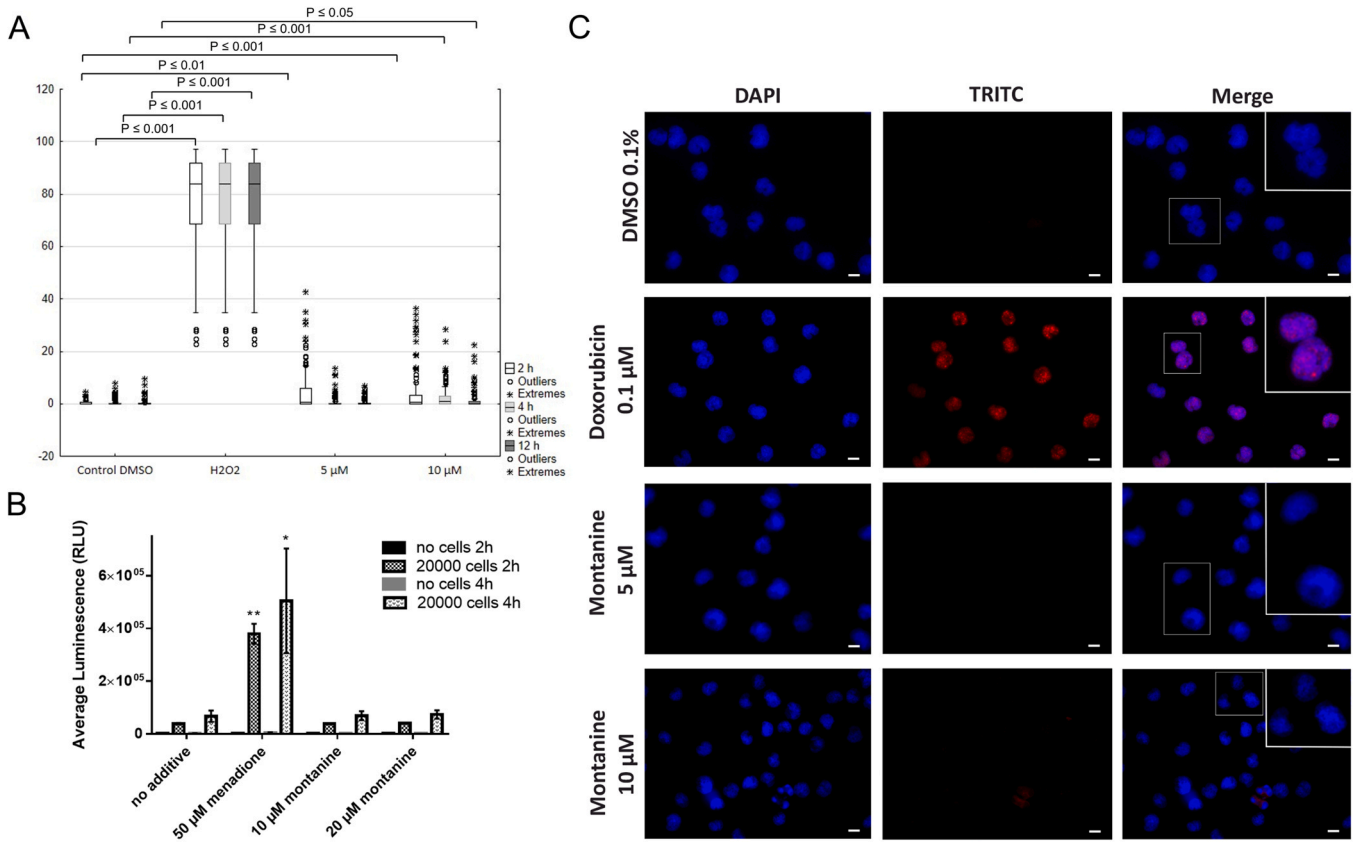


**Fig. 7.** Genotoxic effect of montanine in MOLT-4 cells. (A) An alkaline comet assay was used for the detection of single-strand DNA breaks at 2 h, 4 h and 12 h following treatment with montanine at 5 µM and 10 µM. In addition, 3% hydrogen peroxide was used as the positive DNA damaging control to verify the comet assay. The dark central bar in each box shows the median value; the bottom and top of the box indicate the lower (25%) and upper (75%) quartiles, respectively, and the whiskers represent values within the 1.5 interquartile ranges (values outside this range (outliers) are plotted as solid circles, and extreme values are depicted as asterisks). (B) Luminescence levels (proportional to $H_2O_2$ levels) measured by the ROS-Glo™ $H_2O_2$ assay in cells after 2 h and 4 h of treatment with montanine at 10 µM and 20 µM. Negative controls were treated with the vehicle (0.1% DMSO) used for diluting the tested compound and the positive controls were treated with menadione (50 µM). The bar graph displays the mean ± SD of experiments that were repeated independently for a minimum of three times. * $p < 0.05$, * * $p < 0.01$ and * ** $p < 0.001$, *t*-test. (C) Immunofluorescence γH2AX staining showed that no γH2AX foci formation was changed in the presence of the vehicle control or montanine at 5 µM and 10 µM compared with 0.1 µM doxorubicin-treated positive control, which clearly exhibited increased level of γH2AX protein foci frequency. Experiments were performed in triplicate using epi-fluorescence microscopy. Photographs are representative images from experiments that were repeated independently for a minimum of three times with similar results. Scale bar: 10 µm.

study. Similar to montanine, the alkaloid pancracine, has also been shown to decrease the growth of cancer cell lines, with $IC_{50}$ values ranging from 2.20 µM to 5.08 µM. Montanine has as low $IC_{50}$ value of 1.09 µM for the resistant lung carcinoma A549, and growth-inhibitory activity against this cell line (as measured by real-time proliferation using xCELLigence), which supports its potential to inhibit the growth of dividing tumour cells. A 2.5 µM dose of pancracine showed considerable cytostatic effects on A549 cells within a 48-h treatment interval in the Trypan blue assay, but a 5-times lower dose of montanine (0.5 µM) achieved a similar treatment effect [18]. Compared to the previous results for pancracine, montanine similarly induced a greater number of A549 cells in the G1 phase after treatment with a lower dose of 5 µM. At higher doses of montanine, our cell cycle results for A549 cells indicated alterations in the cell cycle with a decrease in the G1 phase and a concomitant increase in the percentage of cells in the G2 phase. The effect of montanine on the induction of apoptosis was not determined by measuring caspases − 3/ − 7, − 8 and − 9, which was consistent with observations of the effect of pancracine on the A549 cell line.

The effect of pancracine on levels of cell cycle progression-related proteins has been previously described, and we were therefore interested in determining whether montanine also activates the proteins of the signalling cascade leading to G1/S arrest in A549 cells. The key proteins associated with the cell cycle arrest were found to be activated, even after 24 h, although lower concentrations of montanine (2.5 µM and 5 µM) were used compared to those employed for pancracine (10 µM and 20 µM). The signalling pathway appeared to be similarly activated; Akt kinase phosphorylated was downregulated at Thr308 and the p27 protein was upregulated. It is known that cdc25A phosphatase is an essential activator of cell cycle progression and that it is targeted by checkpoint signalling [30]. Cdc25A undergoes phosphorylation during the S phase, resulting in increased phosphatase activity, which is required for entry into the S phase of human cells [31]. This corresponds with our observation: the application of montanine downregulated cdc25A phosphatase after 48 h.

A previous study has shown that ERK1/2 activation promotes cell survival by increasing the levels of anti-apoptotic proteins [32], p38 MAPK is often stimulated by stress or pro-apoptotic factors, and it mediates cell death signalling via p53 phosphorylation, caspase-8 activation, and anti-apoptotic protein inhibition [33]. Our results showed that montanine treatment caused the downregulation of ERK phosphorylation on Thr202/Tyr204 in a time- and concentration-dependent manner, resulting in the upregulation of p38 MAPK phosphorylation on Thr180/Tyr182. These observations agree with our previous finding that treatment with pancracine caused significant activation of p38 MAPK through phosphorylation at Thr180 and Tyr182, and decreased phosphorylation of ERK at Thr202 and Tyr204. The results of previous

work conducted using MOLT-4 cells demonstrated that exposure to 10 μM pancracine for 24 h induced apoptosis, as evidenced by caspases − 3, − 7, − 8 and − 9 activation and by Annexin V staining [18]. Furthermore, pancracine treatment were found to lead to apoptotic cell death in MOLT-4 cells, as marked by the increased protein levels of p53 phosphorylated at Ser392, Bax, p21 and p27, and p38 MAPK phosphorylated at Thr180 and Tyr182 [18]. In our study, we found that montanine dosed at 1 μM for 24 h had a negative impact on MOLT-4 cell viability via apoptosis induction, thus confirming our previous results on montanine-type alkaloids. Furthermore, treatment with 5 μM of montanine caused a significant ($p < 0.001$) change in the mitochondrial membrane potential, which was measured as an early event of apoptosis.

Growing evidence suggests that many conventional chemotherapeutic agents exert anticancer effects by causing DNA damage, which promotes the death of tumour cells via apoptosis [34]. Following genotoxic effects analyses, it was discovered that montanine at a higher evaluated concentration of 10 μM caused ssDNA breaks after 2 h, 4 h and 12 h of treatment. Conversely, neither ROS levels nor γH2AX-positivity in immunofluorescence staining were affected by montanine treatment. Based on Western blot analysis, we found that montanine caused transcriptional upregulation or activation of pro-apoptotic and cell cycle checkpoint proteins, such as p21, Bax, p38 MAPK phosphorylated at Thr180/Tyr182 and Chk1 phosphorylated at Ser345 [35]. The changes in cell cycle kinetics caused by montanine, which increased the proportion of G1 phase cells and decreased the proportion of S-phase cells, were remarkably consistent with previously reported molecular observations. In acute lymphoblastic leukemia cells, another isoquinoline alkaloid of the montanine skeleton-type pancracine, was found to increase the percentage of G1 phase cells and decrease the percentage of S phase [18]. These results are consistent with our findings.

## 5. Conclusions

This study comprehensively compared the anticancer potential of montanine, manthine and 15 montanine analogues. Montanine was found to be the most effective against a battery of cancer cell lines with different tissue origins, surpassing the inhibitory activity of the other montanine-type alkaloids tested. Further mechanistic studies suggested that montanine functioned cytostatically in A549 cells, producing G1-phase accumulation while decreasing the number of S-phase cells, as shown by the downregulation of cdc25A and upregulation of p27. Conversely, MOLT-4 cells demonstrated higher sensitivity to montanine, and death was triggered through apoptosis with caspase activation, mitochondrial depolarisation and Annexin V staining. Moreover, montanine treatment suppressed the proliferation of MOLT-4 cells, and the cells accumulated in the G1 phase of the cell cycle by increasing the protein levels of phosphorylated Chk1 Ser345. These findings show, for the first time, that montanine has powerful cytostatic, cytotoxic and pro-apoptotic activities; therefore, we can conclude that this isoquinoline compound may be a suitable candidate as a chemotherapeutic agent.

## Funding

This work was supported by the project reg. No. CZ.02.1.01/0.0/0.0/18_069/0010046: the Pre-application research into innovative medicines and medical technologies project is co-funded by the European Union. This study was also supported in part by the Cooperatio Program, research area DIAG, and SVV-260543/2020 of the Charles University.

## CRediT authorship contribution statement

Darja Koutova, Negar Maafi, Darina Muthna, Karel Kralovec, Jana Kroustkova, Filip Pidany, Abdul Aziz Timbilla and Radim Havelek performed experiments, analysed data, grafted the figures, tables and wrote the manuscript. Eva Cermakova analysed and synthesized data. Lucie Cahlikova, Radim Havelek and Martina Rezacova designed the study, acquired funding and made revisions to the manuscript. All authors have read and approved the submitted version.

## Declaration of Competing Interest

The authors declare that they have no conflict of interest.

## Acknowledgments

The skilful technical assistance of Mrs Nadezda Mazankova and Mrs Bozena Janska is greatly acknowledged.

## Appendix A. Supporting information

Supplementary data associated with this article can be found in the online version at doi:10.1016/j.biopha.2023.115295.

## References

[1] A.G. Atanasov, S.B. Zotchev, V.M. Dirsch, International natural product sciences taskforce, CT Supuran, Natural products in drug discovery: advances and opportunities, Nat. Rev. Drug Discov. 20 (2021) 200–216, https://doi.org/10.1038/s41573-020-00114-z.

[2] M. Heinrich, J. Mah, V. Amirkia, Alkaloids used as medicines: structural phytochemistry meets biodiversity-an update and forward look, Molecules 26 (2021) 1836, https://doi.org/10.3390/molecules26071836.

[3] F. Labanca, J. Ovesnà, L. Milella, *Papaver somniferum* L. taxonomy, uses and new insight in poppy alkaloid pathways, Phytochem. Rev. 17 (2018) 853–871, https://doi.org/10.1007/s11101-018-9563-3.

[4] Z.X. Qing, J.L. Huang, X.Y. Yang, J.H. Liu, H.L. Cao, F. Xiang, P. Cheng, J.G. Zeng, Anticancer and reversing multidrug resistance activities of natural isoquinoline alkaloids and their structure-activity relationship, Curr. Med. Chem. 25 (2018) 5088–5114, https://doi.org/10.2174/0929867324666170920125135.

[5] D.J. Newman, G.M. Cragg, Natural products as sources of new drugs over the nearly four decades from 01/1981 to 09/2019, J. Nat. Prod. 27 (2020) 770–803, https://doi.org/10.1021/acs.jnatprod.9b01285.

[6] E. Plazas, M.C. Avila M, D.R. Muñoz, L.E.S. Cuca, Natural isoquinoline alkaloids: pharmacological features and multi-target potential for complex diseases, Pharmacol. Res. 177 (2022), 106126, https://doi.org/10.1016/j.phrs.2022.106126.

[7] N. Khaiwa, N.R. Maarouf, M.H. Darwish, D.W.M. Alhamad, A. Sebastian, M. Hamad, H.A. Omar, G. Orive, T.H. Al-Tel, Camptothecin's journey from discovery to WHO Essential Medicine: fifty years of promise, Eur. J. Med. Chem. 223 (2021), 113639, https://doi.org/10.1016/j.ejmech.2021.113639.

[8] A.S. Choudhari, P.C. Mandave, M. Deshpande, P. Ranjekar, O. Prakash, Phytochemicals in cancer treatment: from preclinical studies to clinical practice, Front. Pharmacol. 10 (2020), 1614, https://doi.org/10.3389/fphar.2019.01614.

[9] M.S. Butler, Natural products to drugs: natural product-derived compounds in clinical trials, Nat. Prod. Rep. 25 (2008) 475–516, https://doi.org/10.1039/B402985M.

[10] I. Desgagné-Penix, Biosynthesis of alkaloids in Amaryllidaceae plants: a review, Phytochem Rev. 20 (2021) 409–431, https://doi.org/10.1007/s11101-020-09678-5.

[11] K. Habartová, L. Cahlíková, M. Řezáčová, R. Havelek, The biological activity of alkaloids from the amaryllidaceae: from cholinesterases inhibition to anticancer activity, Nat. Prod. Commun. 11 (2016) 1587–1594, https://doi.org/10.1177/1934578×1601101038.

[12] D. Koutová, N. Maafi, R. Havelek, L. Opletal, G. Blunden, M. Řezáčová, L. Cahlíková, Chemical and biological aspects of montanine-type alkaloids isolated from plants of the amaryllidaceae family, Molecules 25 (2020) 2337, https://doi.org/10.3390/molecules25102337.

[13] L. Cahlíková, I. Kawano, M. Řezáčová, G. Blunden, D. Hulcová, R. Havelek, The Amaryllidaceae alkaloids haemanthamine, haemanthidine and their semisynthetic derivatives as potential drugs, Phytochem. Rev. 20 (2021) 303–323, https://doi.org/10.1007/s11101-020-09675-8.

[14] J.J. Nair, J. van Staden, Cytotoxic agents in the minor alkaloid groups of the amaryllidaceae, Planta Med 87 (2021) 916–936, https://doi.org/10.1055/a-1380–1888.

[15] W.C. Wildman, C.J. Kaufman, Alkaloids of the Amaryllidaceae. III. Isolation of five new alkaloids from *Haemanthus* species, J. Am. Chem. Soc. 77 (1955) 1248–1252, https://doi.org/10.1021/ja01610a045.

[16] J.C. Cedrón, Á.G. Ravelo, L.G. León, J.M. Padrón, A. Estévez-Braun, Antiproliferative and structure activity relationships of amaryllidaceae alkaloids, Molecules 20 (2015) 13854–13863, https://doi.org/10.3390/molecules200813854.

[17] K. Breiterová, D. Koutová, J. Maříková, R. Havelek, J. Kuneš, M. Majorošová, L. Opletal, A. Hošťálková, J. Jenčo, M. Řezáčová, L. Cahlíková, Amaryllidaceae alkaloids of different structural types from *Narcissus* L. cv. Professor einstein and

their cytotoxic activity, Plants 9 (2020) 137, https://doi.org/10.3390/plants9020137.
[18] D. Koutová, R. Havelek, E. Peterová, D. Muthná, K. Královec, K. Breiterová, L. Cahlíková, M. Řezáčová, Pancracine, a montanine-type amaryllidaceae alkaloid, inhibits proliferation of A549 lung adenocarcinoma cells and induces apoptotic cell death in MOLT-4 leukemic cells, Int. J. Mol. Sci. 22 (2021) 7014, https://doi.org/10.3390/ijms22137014.
[19] A.F. Silva, J.P. de Andrade, K.R. Machado, A.B. Rocha, M.A. Apel, M.E. Sobral, A. T. Henriques, J.A. Zuanazzi, Screening for cytotoxic activity of extracts and isolated alkaloids from bulbs of *Hippeastrum vittatum*, Phytomedicine 15 (2008) 882–885, https://doi.org/10.1016/j.phymed.2007.12.001.
[20] M. Masi, S. Van Slambrouck, S. Gunawardana, M.J. van Rensburg, P.C. James, J. G. Mochel, P.S. Heliso, A.S. Albalawi, A. Cimmino, W.A.L. van Otterlo, A. Kornienko, I.R. Green, A. Evidente, Alkaloids isolated from *Haemanthus humilis* Jacq., an indigenous South African Amaryllidaceae: Anticancer activity of coccinine and montanine, S. Afr. J. Bot. 126 (2019) 277–281, https://doi.org/10.1016/j.sajb.2019.01.036.
[21] L. Al Shammari, A. Al Mamun, D. Koutová, M. Majorošová, D. Hulcová, M. Šafratová, K. Breiterová, J. Maříková, R. Havelek, L. Cahlíková, Alkaloid profiling of *Hippeastrum* cultivars by GC-MS, isolation of Amaryllidaceae alkaloids and evaluation of their cytotoxicity, Rec. Nat. Prod. 14 (2020) 154–159, https://doi.org/10.25135/rnp.147.19.06.1302.
[22] K. Govindaraju, A. Ingels, M.N. Hasan, D. Sun, V. Mathieu, M. Masi, A. Evidente, A. Kornienko, Synthetic analogues of the montanine-type alkaloids with activity against apoptosis-resistant cancer cells, Bioorg. Med. Chem. Lett. 28 (2018) 589–593, https://doi.org/10.1016/j.bmcl.2018.01.041.
[23] N. Maafi, F. Pidaný, J. Maříková, J. Korábečný, D. Hulcová, T. Kučera, M. Schmidt, L.Al Shammari, M. Špulák, M.C. Catapano, M. Mecava, L. Prchal, J. Kuneš, J. Janoušek, E. Kohelová, J. Jenčo, L. Nováková, L. Cahlíková, Derivatives of montanine-type alkaloids and their implication for the treatment of Alzheimer's disease: Synthesis, biological activity and in silico study, Bioorg. Med. Chem. Lett. 51 (2021), 128374, https://doi.org/10.1016/j.bmcl.2021.128374.
[24] A.W. Hong, T.H. Cheng, V. Raghukumar, C.K. Sha, An expedient route to Montanine-type Amaryllidaceae alkaloids: total syntheses of (-)-brunsvigine and (-)-manthine, J. Org. Chem. 73 (2008) 7580–7585, https://doi.org/10.1021/jo801089y.
[25] L. Al Shammari, D. Hulcová, J. Maříková, T. Kučera, M. Šafratová, L. Nováková, M. Schmidt, L. Pulkrábková, J. Janoušek, O. Soukup, J. Kuneš, L. Opletal, L. Cahlíková, Amaryllidaceae alkaloids from *Hippeastrum* X *Hybridum* CV. Ferrari, and preparation of vittatine derivatives as potential ligands for Alzheimer´s disease, S. Afr. J. Bot. 136 (2021) 137–146, https://doi.org/10.1016/j.sajb.2020.06.024.
[26] E. Kohelová, J. Maříková, J. Korábečný, D. Hulcová, T. Kučera, D. Jun, J. Chlebek, J. Jenčo, M. Šafratová, M. Hrabinová, A. Ritomská, M. Malaník, R. Peřinová, K. Breiterová, J. Kuneš, L. Nováková, L. Opletal, L. Cahlíková, Alkaloids of *Zephyrantes citrina* (Amaryllidaceae) and their implication to Alzheimer's disease: isolation, structural elucidation and biological activity, Bioorg. Chem. 107 (2021), 104567, https://doi.org/10.1016/j.bioorg.2020.104567.
[27] C. Mei, L. Lei, L.M. Tan, X.J. Xu, B.M. He, C. Luo, J.Y. Yin, X. Li, W. Zhang, H. H. Zhou, Z.Q. Liu, The role of single strand break repair pathways in cellular responses to camptothecin induced DNA damage, Biomed. Pharmacother. 125 (2020), 109875, https://doi.org/10.1016/j.biopha.2020.109875.
[28] H.Y. Min, H.Y. Lee, Mechanisms of resistance to chemotherapy in non-small cell lung cancer, Arch. Pharm. Res. 44 (2021) 146–164, https://doi.org/10.1007/s12272-021-01312-y.
[29] J.C. Cedrón, A. Estévez-Braun, A.G. Ravelo, D. Gutiérrez, N. Flores, M.A. Bucio, N. Pérez-Hernández, P. Joseph-Nathan, Bioactive montanine derivatives from halide-induced rearrangements of haemanthamine-type alkaloids. Absolute configuration by VCD, Org. Lett. 11 (2009) 1491–1494, https://doi.org/10.1021/ol900065x.
[30] L. Busino, M. Chiesa, G.F. Draetta, M. Donzelli, Cdc25A phosphatase: combinatorial phosphorylation, ubiquitylation and proteolysis, Oncogene 23 (2004) 2050–2056, https://doi.org/10.1038/sj.onc.1207394.
[31] I. Hoffmann, G. Draetta, E. Karsenti, Activation of the phosphatase activity of human cdc25A by a cdk2-cyclin E dependent phosphorylation at the G1/S transition, EMBO J. 13 (1994) 4302–4310, https://doi.org/10.1002/j.1460-2075.1994.tb06750.x.
[32] N.J. Darling, S.J. Cook, The role of MAPK signalling pathways in the response to endoplasmic reticulum stress, Biochim. Biophys. Acta Mol. Cell. Res. 1843 (2014) 2150–2163, https://doi.org/10.1016/j.bbamcr.2014.01.009.
[33] J. Yue, J.M. López, Understanding MAPK signaling pathways in apoptosis, Int. J. Mol. Sci. 21 (2020) 2346, https://doi.org/10.3390/ijms21072346.
[34] K. Cheung-Ong, G. Giaever, C. Nislow, DNA-damaging agents in cancer chemotherapy: serendipity and chemical biology, Chem. Biol. 20 (2013) 648–659, https://doi.org/10.1016/j.chembiol.2013.04.007.
[35] J.A. Pietenpol, Z.A. Stewart, Cell cycle checkpoint signaling: cell cycle arrest versus apoptosis, Toxicology 181–182 (2002) 475–481, https://doi.org/10.1016/S0300-483X(02)00460-2.